CHALMERS

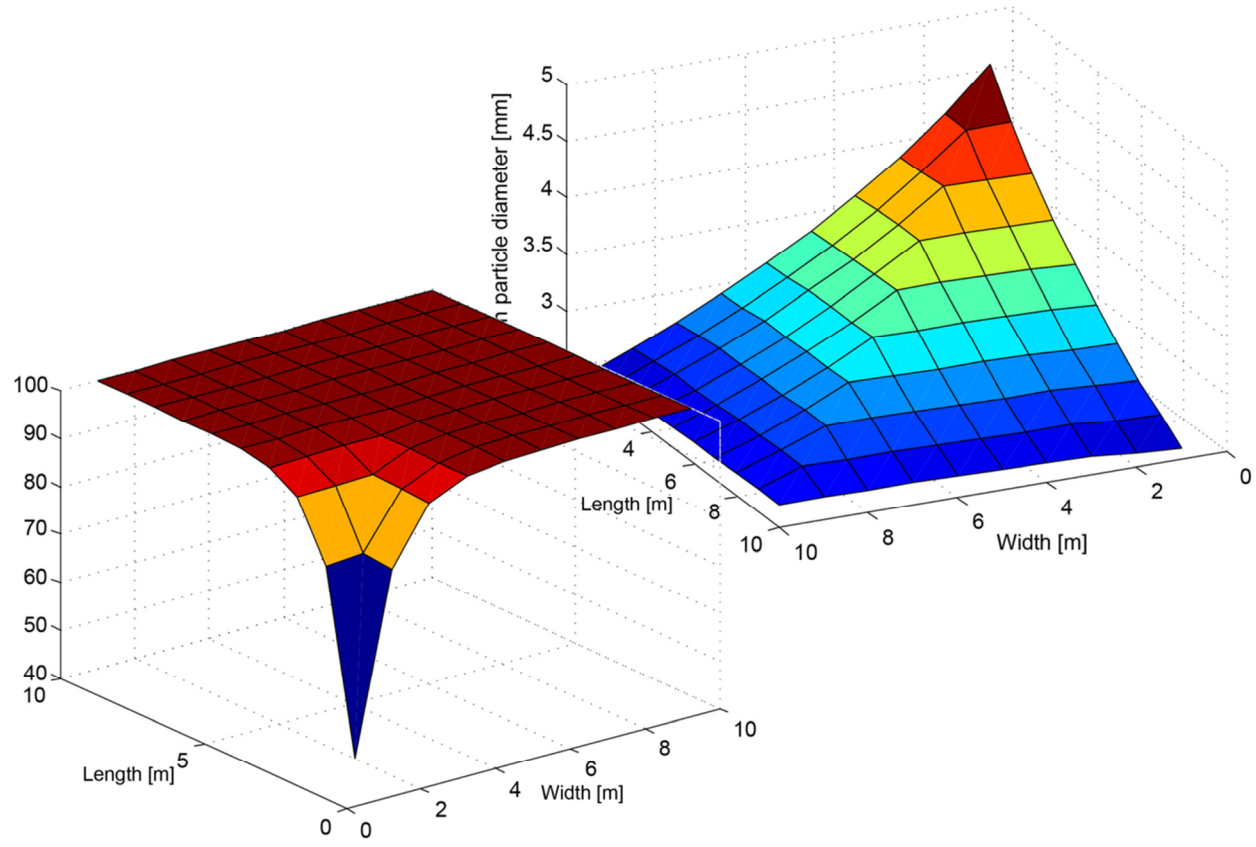

1D Modelling of Fuel Mixing and Conversion in Large-Scale BFB Units

Master's Thesis within the Sustainable Energy Systems programme

GUSTAF LINDBERG

Department of Energy and Environment
Division of Energy Technology
CHALMERS UNIVERSITY OF TECHNOLOGY
Göteborg, Sweden 2013

MASTER'S THESIS

1D Modelling of Fuel Mixing and Conversion in Large-Scale BFB Units

Master's Thesis within the *Sustainable Energy Systems* programme

GUSTAF LINDBERG

SUPERVISOR:
David Pallarès

EXAMINER
David Pallarès

Department of Energy and Environment
Division of Energy Technology
CHALMERS UNIVERSITY OF TECHNOLOGY
Göteborg, Sweden 2013

1D Modelling of Fuel Mixing and Conversion in Large-Scale BFB Units

Master's Thesis within the *Sustainable Energy Systems* programme
GUSTAF LINDBERG

Master's Thesis 2013: T2013-393
Department of Energy and Environment
Division of Energy Technology
Chalmers University of Technology
SE-412 96 Göteborg
Sweden
Telephone: + 46 (0)31-772 1000

Cover: Char conversion and mean particle diameter in the outlet for different sizes for a CLC fuel reactor with a constant cross-sectional specific loading of 4 MW/m^2. The figure is mirrored along the diagonal.

Chalmers Reproservice
Göteborg, Sweden 2013

1D Modelling of Fuel Mixing and Conversion in Large-Scale BFB Units

Master's Thesis in the *Sustainable Energy Systems* programme

GUSTAF LINDBERG
Department of Energy and Environment
Division of Energy Technology
Chalmers University of Technology

ABSTRACT

A one-dimensional model for fuel mixing and conversion in a bubbling fluidized bed has been developed. The model includes fuel particle size development and calculates the concentration profile for char, volatiles, moisture and ash as well as the fuel particle size distribution. Three different kinds of units have been modelled: gasification, combustion and chemical-looping combustion. Two types of fuels, wood and coal, have been used.

Based on the results from the model, the addition of a fragmentation sub-model is very important to fully characterize the char composition in the outlet and the inclusion of particle size classes and particle size development has a large effect on the result. The model presents convergence problems for certain combinations of inputs, such as combustion of fragmenting wood. The model results are sensitive to the value of many inputs such as fuel specific parameters regarding fragmentation and reaction kinetics. Because of these inputs, the use of the model for non-characterized fuels can only be of more qualitative than quantitative use.

Key words: bubbling fluidized bed (BFB), modelling, fuel mixing, gasification, combustion, chemical-looping combustion (CLC), computation fluid dynamics (CFD)

1D-modellering av bränsleomblandning och omvandling i storskaliga BFB-enheter

Examensarbete inom masterprogrammet *Sustainable Energy Systems*
GUSTAF LINDBERG
Institutionen för Energi och Miljö
Avdelningen för Energiteknik
Chalmers tekniska högskola

SAMMANFATTNING

En endimensionell modell för bränsleomblandning och bränsleomvandling i en bubblande fluidiserad bädd har tagits fram. Modellen innehåller storleksutvecklingen för bränslepartiklarna och beräknar även koncentrationsprofilen för koks, flyktiga ämnen, fukt och aska samt bränslets storleksklassfördelning. Tre olika typer av enheter har modellerats: förgasning, förbränning och chemical-looping combustion. Två olika bränslen, trä och kol, har använts.

Baserat på resultaten från modellen så är en modell för fragmentering av bränslet väldigt viktig för att karakterisera kokssammansättningen i utloppet fullt ut och inkluderingen av storleksklasser och storleksutveckling för bränslet har en stor påverkan på resultatet. Modellen visar problem med konvergens vid vissa kombinationer av indata, till exempel förbränning av fragmenterande trä. Modelresultaten är känsliga för värdet på många indata såsom bränslespecifika parametrar för fragmentering och reaktionskinetik. På grund av dessa indata kan resultaten från modellen med okarakteriserade bränslen anses vara mer kvalitativa än kvantitativa.

Nyckelord: bubblande fluidiserad bädd (BFB), modellering, bränsleomblandning, förgasning, förbränning, chemical-looping combustion (CLC), computation fluid dynamics (CFD)

Contents

ABSTRACT I

SAMMANFATTNING II

CONTENTS III

ACKNOWLEDGMENT V

NOTATIONS VI

1 INTRODUCTION 1

1.1 Background 1
1.1.1 Fluidization 1
1.1.2 Gasification 1
1.1.3 Combustion 2
1.1.4 Chemical-Looping combustion 2

1.2 Aim 2

1.3 Scope 2

2 THEORY 3

2.1 CFD and mathematical modelling 3
2.1.1 Velocity field and slip factor 5

2.2 Fuel conversion 6

2.3 Particle size development 8
2.3.1 Fuel conversion 9
2.3.2 Primary fragmentation 10
2.3.3 Secondary fragmentation 11
2.3.4 Attrition 12
2.3.5 Mean particle size 13

2.4 Theory linkup into a model 13
2.4.1 Simulation setups 15

3 METHOD 17

4 RESULTS AND DISCUSSION 18

4.1 Study of the model 18
4.1.1 Mesh independency 18
4.1.2 Number of particle size classes 19
4.1.3 Mean particle diameter 22

4.2 Sensitivity analysis 24
4.2.1 Error tolerance level 24
4.2.2 Temperature profile 25
4.2.3 Activation energy 25
4.2.4 Attrition 28
4.2.5 Fragmentation 29

4.2.6 Slip factor for fuel velocity 30
4.2.7 Dispersion coefficient 32
4.2.8 Particle size distribution 34
4.3 Modelling results 34
4.4 Gasification 37
4.5 Combustion 40
4.6 CLC 41

5 CONCLUSIONS 44

6 FURTHER WORK 45

7 BIBLIOGRAPHY 46

Acknowledgment

I would like to thank:

My supervisor, David Pallarès, for all the help and patience.

Louise Lundberg, for putting up with all my silly questions.

Erik Sette, for supplying numbers and measurements.

Joakim Larsson, for finding the missing minus sign.

Göteborg June 2013

Gustaf Lindberg

Notations

Roman upper case letters

A	Area, m^2
$C_{O_2,\infty}$	Concentration of oxygen in the bulk phase, mol/m^3
C	Concentration in one dimension, kg/m
C_P	Concentration in one dimension at node P, kg/m
D_A	Dispersion coefficient, m^2/s
D_{AB}	Binary diffusion coefficient, m^2/s
E	Activation energy, J/mol
E_c	Attrition rate, kg/s
H	Height, m
L	Length, m
M_c	Molar mass of char, kg/kmol
P_f	Probability of fragmentation
R	Gas constant, J/K mol
T	Temperature, K, °C
U	Fluidization velocity, m/s
V	Volume, m^3
V_{shell}	Volume of one particle size class, m^3
W	Width, m
W_c	Mass of char in the bed, kg

Roman lower case letters

d_{part}	Particle diameter, m
$\bar{d}_m$	Mean particle diameter based on mass fraction, m
$\bar{d}_s$	Sauter mean particle diameter, m
e	Error in mass balance as used for convergence
h_m	Mass transfer coefficient, m/s
$\dot{m}_{bed}$	Mass flow of bed material, kg/s
n_i	Number of particle size classes
$\dot{n}_i$	Number of particles changing class per second, 1/s
k	Attrition rate constant
k_{rC}	Reaction rate constant, m/s
k_{rC0}	Pre-exponential factor, m/s

t	Time, s
t_{dry}	Time of drying and devolatilization, s
u	Velocity, m/s
x	Mass fraction, kg/kg

Greek letters

α	Velocity slip factor
ν	Kinematic viscosity, m^2/s
ρ	Density, kg/m^3
σ	Standard deviation
Ω	Stoichiometric ratio of moles of carbon per mole of oxygen

Subscripts

bed	Bed material
eff	Effective
c	Char
E	Eastern node
e	Eastern face
i	Particle size class
$part$	Particle
W	Western node
w	Western face

Abbreviations

BFB	Bubbling Fluidized Bed
CLC	Chemical-Looping Combustion
CLOU	Chemical-Looping with Oxygen Uncoupling
PDF	Probability Density Function
PSD	Particle Size Distribution

Dimensionless numbers

Pe	Péclet
Re	Reynolds
Sc	Schmidt
Sh	Sherwood

1 Introduction

1.1 Background

The fate of fuel particles strongly affects the overall performance of a fluidized bed unit. To make an accurate, comprehensive model of a large scale fluidized bed unit, a proper representation of the fuel mixing is needed. The industry is looking for such a comprehensive model for use in the design of new units as well as modifications and optimizations of existing units.

Many different physical processes affect the fuel mixing. The fluid dynamical problem of where fuel particles move in a gas-solid suspension becomes more complex as fuel particles are also undergoing changes in their physical properties and composition as they convert, due to drying, devolatilization, combustion, attrition and fragmentation. All these processes are connected making fuel mixing and conversion a complex problem to solve.

1.1.1 Fluidization

Fluidization means suspending a bed material and fuel in an airflow during the fuel conversion process. The fluidization makes the bed act like a bubbling fluid which has given it the name, bubbling fluidized bed (BFB). The high degree of mixing in the fluidized bed leads to high heat transfer which in turn makes in suitable for a wide range of fuels with varying heat content. This property is of interest for developing co-combustion units where the same combustor can take a mix of fuel like coal, wood and household waste. Another property of the bed is the inherent SO_x emission control since limestone can be added directly to the bed, which absorbs sulphur at the site of combustion instead of relying on flue gas cleaning.

1.1.2 Gasification

In a gasifier, the coal in the fuel reacts with water in the form of steam to form carbon monoxide and hydrogen gas, also known as syngas, according to (1).

$$C + H_2O \rightarrow CO + H_2 \tag{1}$$

The produced syngas can either be burned as a replacement for natural gas or it can be used as a raw material for further processing. It can, for example, be used to produce liquid fuels with the Fischer-Tropsch process. If the fuel is biomass, gasification can be used to create a carbon dioxide neutral fuel.

Chalmers has a 2 MW research gasifier which is used in this work as a reference unit for gasification. Further information is available in the literature. (Larsson & Olsson 2013) (Thunman & Seemann 2009)

A large scale gasification plant, GoBiGas, is being built in Gothenburg. The first step which is projected to produce 20 MW of bio-gas is planned to be finished in 2013 and the second, larger, step of 80 MW is planned to be finished in 2016. The plant will have a methanisation step that converts the syngas from gasification to methane which will be distributed through the existing natural gas grid. The fuel will be residue from the forest industry which means that the produced bio-gas will be carbon neutral. (Energi n.d.)

Modelling of the gasification process is important in order to estimate the char conversion and help in deciding the size of the gasification unit.

1.1.3 Combustion

In a combustor, char is combusted with oxygen to form carbon dioxide according to:

$$C + O_2 \rightarrow CO_2 \quad (2)$$

Modelling is important in order to properly characterize the fuel conversion process.

1.1.4 Chemical-Looping combustion

Chemical-looping combustion CLC is a system where oxygen from the air is absorbed to an oxygen carrier in one reactor and combustion takes place in another reactor with the reduction on the cited oxygen carrier being the only source of oxidizer. This way, no nitrogen from the air is present at the combustion which creates a flue gas stream that is not diluted by nitrogen. This is one solution to the problem of carbon dioxide separation for carbon capture and storage.

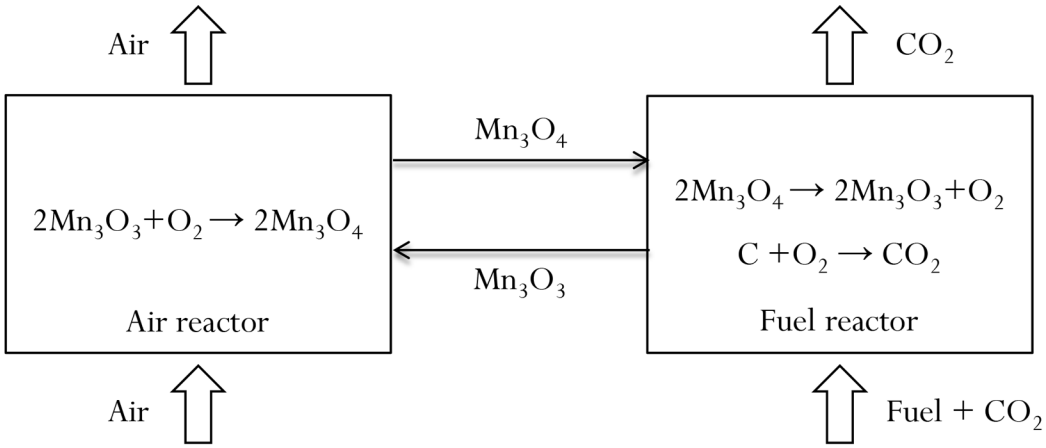

Figure 1 Principal scheme of CLC with carbon as fuel and Mn_3O_4/Mn_3O_3 as oxygen carrier.

In addition to modelling the overall conversion, the fuel particle size distribution in the outlet is of great interest in a CLC unit. To prevent fuel from entering the air reactor, a small unit for char burnout, called carbon stripper, can be placed in the stream exiting the fuel reactor. Design and operation of carbon strippers are closely related to the load and particle size distribution of char.

1.2 Aim

The aim of the project is to develop a one-dimensional mathematical model that describes the fuel mixing and conversion in a bubbling fluidized bed and can serve as a tool to identify critical phenomena and variables in the mixing and conversion phenomena. Three specific applications (gasification, combustion and CLC) and two specific fuels (coal and wood) will be considered.

1.3 Scope

Only mass transfer will be considered in this work, i.e. no energy balances are included. A given temperature field over the bed will instead be assumed.

2 Theory

2.1 CFD and mathematical modelling

Computational fluid dynamics, CFD, is a powerful tool to analyse complex problems involving fluid flows. With CFD, a system can be modelled and evaluated without having to conduct any physical experiments. This can save both time and money in both grass root design and retrofitting different kinds of industrial equipment.

The foundation of CFD is the Navier-Stokes equations which describe the transport and conservation of mass (3), momentum (4), species (5) and energy in a flowing fluid.

$$\frac{\partial \rho}{\partial t} = \nabla \rho \boldsymbol{u} \tag{3}$$

$$\frac{\partial}{\partial t}\rho \boldsymbol{u} + \nabla \rho \boldsymbol{u}^2 = -\nabla p + \nabla \tau + \rho g + F \tag{4}$$

$$\frac{\partial \rho}{\partial t} = \boldsymbol{u}\nabla \rho - D_A \nabla^2 \rho + S \tag{5}$$

The left hand side in equation (5) is the accumulation term. The right hand side consists of convection, dispersion and source terms respectively. Dispersion is a macroscopic version of diffusion where the driving force is isotropic lateral solids mixing. Because dispersion is analogous to diffusion, Fick's law, equation (6), can be used to describe it.

$$J = -D_A \frac{\partial \rho}{\partial x} \tag{6}$$

Rewriting the transport equation for mass in one dimension yields equation (7).

$$\frac{\partial \rho}{\partial t} = \boldsymbol{u}\frac{\mathrm{d}\rho}{\mathrm{d}x} - D_A \frac{\mathrm{d}^2 \rho}{\mathrm{d}x^2} + S \tag{7}$$

To solve this differential equation, a finite-volume method was employed which divides it into a set of algebraic equations which can be solved numerically. The first step is to divide the domain into a set of computational cells. Each cell has a node in its centre and is surrounded by its faces. In one dimension each cell has two faces, one east and one west, as illustrated by Figure 2.

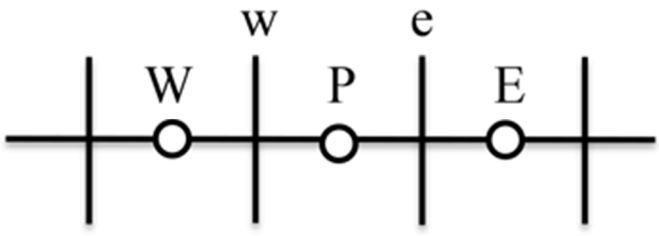

Figure 2 Illustration of a mesh with three cells. The node in the current cell is marked with a P, the node in the western cell W and the eastern E. The faces of the studied cell are marked with w and e respectively.

The transport equation can now be integrated with the cell as a control volume which combined with a steady state assumption where the accumulation term is set to zero yields equation (8).

$$0 = (uC)_{\mathrm{e}} - (uC)_w + \left(D_A \frac{\mathrm{d}C}{\mathrm{d}x}\right)_{\mathrm{e}} - \left(D_A \frac{\mathrm{d}C}{\mathrm{d}x}\right)_{\mathrm{w}} + S \tag{8}$$

To solve equation (8), an estimation of the concentration gradient is needed as well as the value of the concentration at the faces. The concentration gradient can be estimated by a first order Taylor expansion shown in equation (9).

$$\left(\frac{\mathrm{d}C}{\mathrm{d}x}\right)_w = \frac{C_P - C_W}{x_P - x_W}, \qquad \left(\frac{\mathrm{d}C}{\mathrm{d}x}\right)_e = \frac{C_E - C_P}{x_E - x_P} \tag{9}$$

There are several discretization schemes to estimate the concentration at the faces. The two simplest are central differencing which takes a mean value for the two neighbouring cells, equation (10), and first-order upwind which assumes that the concentration at the face is the same as the concentration at the upwind cell, equation (11).

$$C_w = \frac{C_W + C_P}{2}, \qquad \mathrm{C_e} = \frac{C_E + C_P}{2} \tag{10}$$

$$C_w = C_W, \qquad C_e = C_P \tag{11}$$

The central differencing scheme is bounded which means that the calculated value of the face cannot be larger or smaller than the values of the cells surrounding it which gives it an inherent stability. However, it lacks transportiveness which means it does not inherently know the direction of flow which in strong convective cases can lead to diverging solutions. First-order upwind is both bounded and it fulfils the requirement for transportiveness but it can introduce numerical errors if the flow is not strongly convective. To use the positive properties of both schemes, a hybrid scheme is used where different schemes are chosen for each cell depending on the conditions in that particular cell. To evaluate which transport process, convection or dispersion, that is dominant, the Péclet number is calculated for all nodes.

$$Pe = \frac{\Delta x u}{D_A} \tag{12}$$

If $|Pe| > 2$, convection is dominating and first-order upwind is used. If on the other hand, $|Pe| < 2$, dispersion is dominating and central differencing is used.

Now, the transport equation can be written as equation (13) for central differencing and equation (14) for first-order upwind.

$$0 = u\frac{C_W + C_P}{2} - u\frac{C_P + C_E}{2} - D_A\frac{C_P - C_W}{\Delta x_w} - D_A\frac{C_P - C_E}{\Delta x_E} + S \tag{13}$$

$$0 = uC_W - uC_P - D_A\frac{C_P - C_W}{\Delta x_w} - D_A\frac{C_P - C_E}{\Delta x_E} + S \tag{14}$$

Since the only difference between the two lies in the discretization of the convective term, only the first-order upwind will be shown hereafter in order to save space. Equations (13) and (14) can now be solved for node P if the value of the concentration is known in nodes W and E. To solve the system of equation generated, the Gauss-

Seidel method is used. First, a concentration is guessed for all nodes. Then the concentration in node P can be calculated based on the initial guessed concentration in node W and E. Moving to the next node, the former node E becomes the new node P. Then the concentration in this new P can be calculated based on the initial guess in node E and the previously calculated value in node W. The first and last nodes need some special attention since they only have one neighbouring node. To solve this, two extra nodes are introduced at the faces at the walls, as illustrated in Figure 3. They are known as shadow nodes and are set to have the same value as the first and last node respectively. This is done to fulfil the boundary condition of no mass transport across the walls.

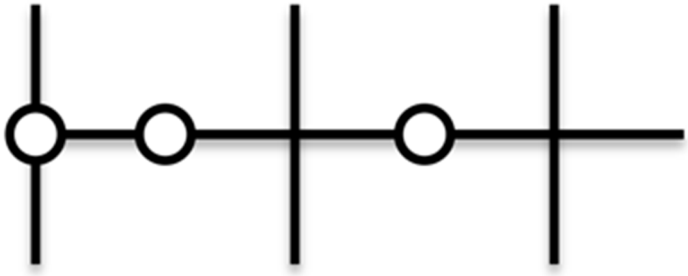

Figure 3 Illustration of the shadow node at the wall of the mesh.

All the nodes are iterated through once and are then compared to a convergence criterion. If it is fulfilled, the solution is assumed to be converged and if not, one starts over from the first node and iterate through them again. This process is repeated until a converged solution is found.

The simplest source term for a system with no reactions is an inlet flow and an exit flow, forming a source and a sink for the system. In this model, the source term for char is shown in equation (15) and is only applied to the cells corresponding to the inlet port. It is assumed that fuel and bed material enter through the same port.

$$S_{feed} = \frac{\dot{m}_{feed}}{L_{feed}} \cdot \Delta x \tag{15}$$

The outlet was modelled using an outlet velocity multiplied with the concentration in the current cell as shown in equation (16).

$$S_{outlet} = C_P u_{exit} \tag{16}$$

The overall mass balance for a system with convection, dispersion, one sink and one source term but no reaction is shown in equation (17).

$$0 = uC_W - uC_P - D_A \frac{C_P - C_W}{\Delta x_w} - D_A \frac{C_P - C_E}{\Delta x_E} + \frac{\dot{m}_{feed}}{L_{feed}} \cdot \Delta x - C_P u_{exit} \tag{17}$$

2.1.1 Velocity field and slip factor

Fuel particles are assumed to follow the flow of the bed material in the unit. The velocity field for the particles is therefore solved by a mass balance for the bed material as shown in equation (18). The exit velocity is solved in the same way.

$$u = \frac{\dot{m}_{bed}}{\rho_{bed} H_{bed} W_{bed}} \tag{18}$$

The velocity is assumed to be constant between the inlet and outlet in the bed and it is assumed to be zero elsewhere. Over the inlet and outlet, the velocity profile is assumed to vary linearly as illustrated in Figure 4.

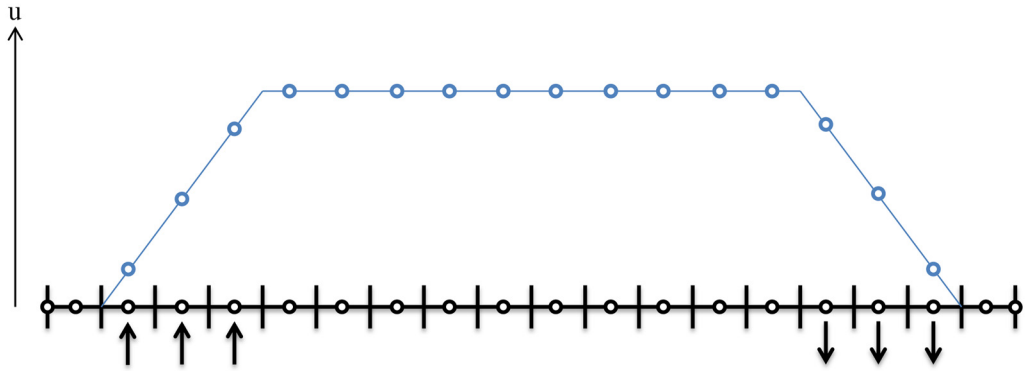

Figure 4 Illustration of the velocity field with the mesh and nodes in black and the velocity field and the values in the nodes in blue. The arrows mark the inlet and outlet.

However, fuel particles will not always follow the flow of the bed material. Larger particles are not as likely to follow the flow of the bed material as small particles. To compensate for this, a slip velocity for the particles is calculated by multiplying the bed solids velocity by a slip factor α.

$$0 = \alpha u C_W - \alpha u C_P - D_A \frac{C_P - C_W}{\Delta x_w} - D_A \frac{C_P - C_E}{\Delta x_E} + \frac{\dot{m}_{feed}}{L_{feed}} \cdot \Delta x - C_P \alpha u_{exit} \tag{19}$$

It is defined so that $\alpha = 1$ when the particles follow the velocity field perfectly and $\alpha = 0$ when the particles do not follow the velocity field at all. In the model, the slip velocity factor is assumed to be linear between 0.6 for the largest particle to 1 for the smallest (Larsson & Olsson 2013).

2.2 Fuel conversion

The fuel conversion can be divided into four distinct steps; heat up, drying, devolatilization and char conversion. For a thermally small particle, these steps happen sequentially so the drying starts after the particle is heated and the devolatilization starts after the particle is dried and so on. For a thermally large particle, which is considered in this work, the steps happen in parallel, so as the surface of a coal particle experiences char conversion, the core can still be drying. This is caused by the temperature gradient formed in larger particles. The limited heat transfer inhibit drying and devolatilization of the inner parts of the particle. Due to the high surrounding temperature and the short time of heating compared to the time of drying and devolatilization, the time needed for heat up to the evaporation temperature is neglected. The time needed for drying and devolatilization of a thermally large particle can be calculated with equation (20).

$$t_{dry/devol} = 12.08 \cdot 10^7 d_{part}^{1.44} T^{-1.66} \quad (20)$$

The rate of char combustion can be described by equation (21). For char gasification, the concentration of oxygen is replaced with the concentration of steam.

$$\rho_c \frac{\mathrm{d}V}{\mathrm{d}t} = -\Omega A k_{rC,eff} C_{O_2,\infty} M_c \quad (21)$$

The effective reaction rate constant is given by equation (22) which includes both kinetics and diffusion.

$$k_{rC,eff} = \frac{k_{rC} h_m}{k_{rC} + h_m} \quad (22)$$

The mass transfer coefficient is obtained from the Sherwood number which is turn is a function of the Reynolds and Schmidt numbers.

$$h_m = \frac{D_{AB} Sh}{d} \quad (23)$$

$$Sh = \left(2 + 0.6 Re^{0.5} Sc^{\frac{1}{3}}\right) \cdot 0.9 \quad (24)$$

$$Re = \frac{d_{part} u}{\nu} \quad (25)$$

$$Sc = \frac{\nu}{D_{AB}} \quad (26)$$

The reaction rate constant is given by the Arrhenius expression.

$$k_{rC} = k_{rC0} e^{-E/RT} \quad (27)$$

The pre-exponential factor can in turn be expressed as a function of the activation energy as shown in equation (28).

$$k_{rC0} = 10^{(0.2 \cdot 10^{-4} E + 2)} \quad (28)$$

The time for a large char particle to completely burn out can be estimated according to equation (29).

$$t_{burn} = \frac{\rho_c d_{part}^2}{8 \Omega D_{AB} C_{O_2,\infty} M_c} \quad (29)$$

Knowing this, a critical length representing the shortest dimensions for a unit for complete fuel conversion can be estimated, making use of the Einstein (1953) equation.

$$L_{crit} = \sqrt{2 t_{burn} D_A} \quad (30)$$

In the model, equation (21) is implemented to describe the char conversion. Since equation (21) is written as reaction rate for one particle, it needs to be scaled for the total fuel area in each cell i.e.

$$S_{conversion} = -\Omega A_{part} \frac{C_P \Delta x}{\rho_c V_{part}} k_{rC,eff} C_{O_2,\infty} M_c \quad (31)$$

Equation (31) can be conveniently expressed as:

$$S_{conversion} = -r^* C_P \quad (32)$$

Where:

$$r^* = \Omega A_{part} \frac{\Delta x}{\rho_c V_{part}} k_{rC,eff} C_{O_2,\infty} M_c \quad (33)$$

2.3 Particle size development

This work considers three main processes that cause the fuel particle size to change in the conversion process: fragmentation, attrition and reduction due to fuel conversion. The first two of these are collectively called comminution and the fragmentation is divided into primary and secondary fragmentation.

To model the size decrease by char conversion, the fuel particles are divided into a set of discrete size classes, i, which are numbered from the largest to the smallest. The classes are divided so that each class contains the same amount of mass, which together with the assumption that the fuel particles are spherical and that the density is constant throughout the particle, yields that every particle size class will have the same volume according to:

$$V_{shell} = \frac{V_{part}}{n_i} \quad (34)$$

To get a mean radius for each size class, node points are defined in each size class in the same way, i.e. all node classes contain the same mass except for the smallest one which is half the size. These nodes are used to evaluate a mean particle radius for the fuel conversion properties. The particle size classes are illustrated in Figure 5.

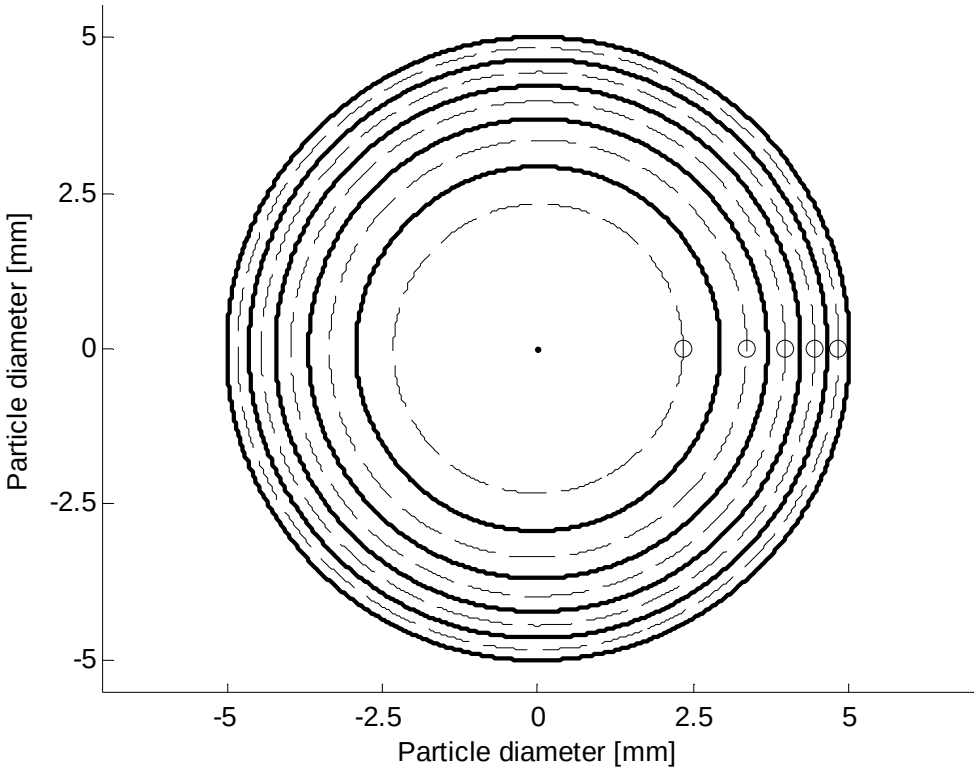

Figure 5 An illustration of the particle size classes for a particle with a diameter of 10 mm divided into five size classes. The solid lines show the size classes and the dashed lines with the circles show the nodes.

As can been seen in Figure 5, an inherent problem with choosing the sizes based on constant mass is that the larger size classes are very close together and the smallest size class is rather large in comparison to the largest. In the illustrated example, the smallest particle has more than half the diameter of the largest. To achieve a more accurate result for smaller particles, the number of particle size classes needs to be large. In the model, 300 particle size classes are used which mean that the smallest class diameter is 1.5 mm if the largest is 10 mm.

2.3.1 Fuel conversion

As the outermost shell of the fuel particle is converted into gas, the size decreases according to the shrinking sphere combustion model. As the particle decreases in size, it changes size class. This is added to the model by rewriting the source term for fuel conversion, equation (31), so it becomes one sink in size class i for particles shrinking to size class $i+1$ and one source for particles entering from size class $i-1$. Thus, the model is based around the number of particles being constant throughout conversion so the number of particles leaving one size class is the same number entering the next and the difference in mass is the amount that has been converted to gas. One further assumption is made that the particles shrink no more than one size class in a given cell. With this, a balance for cell P and size class i can be set up.

$$r_i^* C_{P,i} = \dot{n}_i V_{shell} \rho_c \tag{35}$$

$$\dot{n}_i = \frac{r_i^* C_{P,i}}{V_{shell}\rho_c} \tag{36}$$

Here, equation (33) is rewritten to account for particle size classes.

$$r_i^* = \Omega A_i \frac{\Delta x}{\rho_c V_i} k_{rC,eff} C_{O_2,\infty} M_c \tag{37}$$

The total amount of mass that leaves particle size class i can be expressed as:

$$\dot{m}_c = \dot{n}_i V_i \rho_c \tag{38}$$

When equation (36) and (38) are combined, an expression for the source term for the sink in particle size class *i* and node P is found.

$$S_{conversion\ sink} = r_i^* \frac{V_i}{V_{shell}} C_{P,i} \tag{39}$$

The source term for particle entering size class *i* from a larger size is derived in the same way yielding.

$$S_{conversion\ source} = r_{i-1}^* \frac{V_i}{V_{shell}} C_{P,i-1} \tag{40}$$

2.3.2 Primary fragmentation

Primary fragmentation takes place during drying and devolatilization when fuel particles are subjected to high thermal stress and a rapid build-up of internal pressure as water vapour and volatiles are released as the particle is heated. This combined with mechanical stress causes the fuel particles to break into smaller pieces. The process is very fast and highly dependent on particle size and both the type and composition of the fuel.

Primary fragmentation can be modelled based on a probability of fragmentation and an average number of fragments generated. This approach requires two empirical, fuel specific constants which can be found in the literature. In this work, the fragmentation probability for South African bituminous coal was taken from the work of Chirone *et al.* (Chirone 1991).

No values for the probability of fragmentation were found for wood in the literature so a statistical model (Thunman 1997), was chosen instead

$$P_f = 1 - \exp(-0.11 \cdot t_{dry}) \tag{41}$$

The average number of fragments created was taken from literature and is shown in Table 1. (Scala & Chirone 2006) (Sudhakar et al. 2008)

Table 1 Probability of fragmentation and average number of fragments created for primary fragmentation of wood and coal.

Wood			Coal		
Diameter [mm]	P_f	Number of fragments	Diameter [mm]	P_f	Number of fragments
5.2	-	2.5	1.4	0.005	1.1
15	-	4.5	2.0	0.03	1.2
20	-	5	2.8	0.08	2.0
25	-	11	3.3	0.22	2.0
			4.0	0.2	2.3
			4.7	0.25	2.8
			6.3	0.35	4.6
			9.0	0.6	7.6

The assumption is made that all fragments are the same size and that they are spherical like the mother particle. Furthermore, primary fragmentation is assumed to be an instantaneous process that occurs directly in the feed. This means that it can be modelled by changing the fed particle size distribution from the one given as input, in this work mono sized is assumed, to a new, calculated distribution after primary fragmentation.

2.3.3 Secondary fragmentation

Secondary fragmentation is a slower process which occurs during char conversion. As the char particle undergoes conversion, cracks can appear which make the particle break into pieces. The overall structural integrity of the particle can also be lowered as mass is converted which results in a porous particle that can more easily break due to mechanical stress. Secondary fragmentation is highly dependent on fuel type where char from wood can undergo a significant fragmentation whereas char from coal does not fragment to the same extent. (Chirone 1991)

No probability of fragmentation and average number of fragments for the secondary fragmentation of coal was found in the literature so the fragmentation of coal was modelled using a normal distribution as suggested by Chirone. The mean value was taken to be 5 mm and the standard deviation 0.5 mm. (Chirone, Salatino & Massimilla 1989)

Secondary fragmentation for wood is treated in the same way as primary fragmentation for coal in the model but with other values for the probability of fragmentation and average number of fragments which were taken from the work of Sudhakar as shown in Table 2 (Sudhakar et al. 2008).

Table 2 Probability of fragmentation and average number of fragments created for secondary fragmentation of wood.

Diameter [mm]	P_f	Number of fragments
10	1	2
25	0	6.6

According to Sudhakar, large spherical char particles do not undergo secondary fragmentation. Therefore, the probability of fragmentation for 25 mm char particles is set to zero. The number of fragments is still needed for the interpolation for the intermediate diameters so the value 6.6 was interpolated from the results of Sudhakar for numerical reasons. (Sudhakar et al. 2008)

Secondary fragmentation is only applied to the sub model for char combustion and not to the volatiles or moisture due to the nature of secondary fragmentation. A major assumption is made since secondary fragmentation is added directly at the feed, just like the primary. This is done to avoid having to include another iteration loop to the code. If the secondary fragmentation were to be included at 25-75 % of the burnout time, the particle size distribution at that point would need to be iterated, adding much computational time to the algorithm. Therefore, secondary fragmentation is treated the same as the primary and is added on the output particle size distribution from the sub model for primary fragmentation, before being entered into the sub model for char conversion.

2.3.4 Attrition

Attrition is caused by the mechanical abrasion from the bed material on the char particles which generates a large number of very fine particles and has been modelled by (Chirone 1991) as:

$$E_c = kU\frac{W_c}{d_p} \tag{42}$$

In the model, attrition is handled as a further char conversion reaction alongside the regular fuel conversion. The size of the particles created by attrition is so small that the burnout time is much shorter than the residence time in the computational cell so there is no need to include the transport of those particles in the model. The attrition is scaled after the amount of char in each cell and each particle size class according to equation (43).

$$S_{attrition} = kU\frac{\Delta x}{d_i}C_{p,i} \tag{43}$$

Values for the attrition constant for coal and wood are shown in Table 3 and were taken from the work of Chirone and Scala respectively. (Chirone 1991) (Scala & Chirone 2006)

Table 3 Attrition constant, k, for wood and coal used in the model.

	Wood	Coal
k	$3 \cdot 10^{-7}$	$3.33 \cdot 10^{-8}$

The attrition constant varies with two orders of magnitude in the literature. It is highly dependent on the type of coal which the studied char originates from. The internal structure is important since a porous petroleum coke will be more susceptible to the abrasion of the bed material than solid anthracite. Even more important is the properties of the bed material. A high fluidisation velocity and large silica sand particles results in a higher attrition constant than a lower velocity and a less abrasive bed material. As an example, Arena *et al.* showed that the attrition constant increases with a factor of two, from 5.79 to 12, when the diameter of the silica sand used as bed material was increased from 0.6-0.85 mm to 1.0-1.4 mm (Arena, D'Amore & Massimilla 1983).

2.3.5 Mean particle size

There are many ways to determine a mean size for a particle population consisting of different sizes. In this work, three different mean values for the particle diameter are considered.

A mean diameter based on mass fraction can be expressed as:

$$\bar{d}_m = \sum d_i x_i \tag{44}$$

Another way to determine the mean diameter of a large population is D50 which is defined as the diameter where 50 % of the mass is larger than the D50 diameter and 50 % is lower. It can be calculated as the diameter where the cumulative mass distribution is 0.5.

The third way to characterize particles is the Sauter mean diameter, which is defined as the diameter of a sphere that has the same volume to area ratio as the particles of interest. It is expressed as:

$$\bar{d}_s = \frac{1}{\sum \frac{x_i}{d_i}} \tag{45}$$

2.4 Theory linkup into a model

The transport equation for species can be combined with the different source terms into equation (46), yielding equation (47).

$$\begin{aligned} 0 = {} & convection + dispersion + S_{feed} - S_{outlet} \\ & + S_{conversion\ source} - S_{conversion\ sink} \\ & - S_{attrition} \end{aligned} \tag{46}$$

$$\begin{aligned} 0 = {} & uC_{W,i} - uC_{P,i} - D_A \frac{C_{P,i} - C_{W,i}}{\Delta x_w} - D_A \frac{C_{P,i} - C_{E,i}}{\Delta x_E} + \\ & \frac{\dot{m}_{feed}}{L_{feed}} \cdot \Delta x - C_{P,i} u_{exit} + r^*_{i-1} \frac{V_i}{V_{shell}} C_{P,i-1} - r^* \frac{V_i}{V_{shell}} C_{P,i} \\ & - kU \frac{\Delta x}{d_i} C_{P,i} \end{aligned} \tag{47}$$

To solve equation (47), it is rearranged so terms that depend on the concentration in cell P are on the right hand side and the rest is on the left hand side.

$$
\begin{aligned}
-uC_{W,i} - D_A\frac{C_{W,i}}{\Delta x_W} - D_A\frac{C_{E,i}}{\Delta x_E} - \frac{\dot{m}_{feed}}{L_{feed}}\cdot\Delta x \\
&= -uC_{P,i} - D_A\frac{C_{P,i}}{\Delta x_W} - D_A\frac{C_{P,i}}{\Delta x_E} - C_{P,i}u_{exit} \\
&+ r_{i-1}^*\frac{V_i}{V_{shell}}C_{P,i-1} - r_i^*\frac{V_i}{V_{shell}}C_{P,i} \\
&- kU\frac{\Delta x}{d_i}C_{P,i}
\end{aligned}
\tag{48}
$$

Which is further simplified to:

$$
\begin{aligned}
-uC_{W,i} - D_A\frac{C_{W,i}}{\Delta x_W} - D_A\frac{C_{E,i}}{\Delta x_E} - \frac{\dot{m}_{feed}}{L_{feed}}\cdot\Delta x \\
&= r_{i-1}^*\frac{V_i}{V_{shell}}C_{P,i-1} \\
&+ \left(-u_{exit} - \frac{D_A}{\Delta x_W} - \frac{D_A}{\Delta x_E} - r_i^*\frac{V_i}{V_{shell}}\right. \\
&\left. - kU\frac{\Delta x}{d_i}\right)C_{P,i}
\end{aligned}
\tag{49}
$$

This can be rewritten on matrix form, $Ax = b$.

$$
b = -uC_{W,i} - D_A\frac{C_{W,i}}{\Delta x_W} - D_A\frac{C_{E,i}}{\Delta x_E} - \frac{\dot{m}_{feed}}{L_{feed}}\cdot\Delta x \tag{50}
$$

$$
a_{1,i} = -u_{exit} - \frac{D_A}{\Delta x_W} - \frac{D_A}{\Delta x_E} - r_i^*\frac{V_i}{V_{shell}} - kU\frac{\Delta x}{d_i} \tag{51}
$$

$$
a_{2,i-1} = r_{i-1}^*\frac{V_i}{V_{shell}} \tag{52}
$$

$$
\begin{bmatrix}
a_{1,1} & 0 & & \cdots & 0 \\
a_{2,2} & a_{1,2} & 0 & & \vdots \\
0 & \ddots & \ddots & 0 & \\
\vdots & & a_{2,i-1} & a_{1,i-1} & 0 \\
0 & \cdots & 0 & a_{2,i} & a_{1,i}
\end{bmatrix}
\begin{bmatrix}
C_{P,1} \\ C_{P,2} \\ \vdots \\ C_{P,i-1} \\ C_{P,i}
\end{bmatrix}
=
\begin{bmatrix}
b_1 \\ b_2 \\ \vdots \\ b_{i-1} \\ b_i
\end{bmatrix}
\tag{53}
$$

This system of linear equations is solved for each cell to get the concentration for all particle size classes in cell P in the same way as described previously.

The convergence criterion for char is the overall mass balance divided by a scaling factor which is set to be the char feed rate as shown in equation (54).

$$
e = \frac{\left(S_{feed} - S_{outlet} - S_{conversion} - S_{attrition}\right)}{S_{feed}} \tag{54}
$$

Convergence is assumed to be reached when the error is smaller than 10^{-4}.

When solving the volatiles and moisture species, the terms for conversion and attrition are replaced by a source term for drying and devolatilization.

$$S_{dry/devol} = \frac{\Delta x}{t_{dry/devol}} C_{P,i} \quad (55)$$

The convergence criterion for volatiles and moisture is similar to the one for char but with drying and devolatilization instead of conversion and the attrition term is removed as shown in equation (56).

$$e = \frac{\left(S_{feed} - S_{outlet} - S_{dry/devol}\right)}{S_{feed}} \quad (56)$$

Ash is not solved explicitly. The assumption is made that since the transportation of ash is coupled with the transportation of char, there is no need to solve the transport equation for ash. Instead, the calculated concentration profile for char is scaled based on the amount of ash in the fuel in post processing.

The proximate analysis for the two reference fuels, coal and wood, are taken from Arena and Sudhakar respectively and the lower heating values are taken from an energy technology table. The fuel properties are shown in Table 4. No moisture was reported for the coal so a moisture content of 10 % was assumed and the proximate analysis was recalculated based on that.

Table 4 Fuel properties for coal and wood. The proximate analysis for coal is taken from (Arena, D'Amore & Massimilla 1983), the proximate analysis for wood is taken from (Sudhakar et al. 2008) and the lower heating values are taken from (Mörtstedt & Hellsten 2005).

	Bituminous coal (South African)	Wood (*Casuarina equisetifolia*)
Fixed carbon [%]	54	10.5
Volatiles [%]	22.5	82.6
Moisture [%]	10	6.5
Ash [%]	13.5	0.4
Lower heating value [MJ/kg]	30	13

2.4.1 Simulation setups

Gasification

A reference case for the simulations of a gasifier was chosen based on the Chalmers gasifier. The operational conditions and dimensions were taken from (Larsson & Olsson 2013).

The activation energy is chosen so the overall char conversion matches that of the Chalmers gasifier.

The temperature profile for the gasifier assumes that the temperature is linearly increasing across the unit, from a low value on the inlet side to a high value on the

outlet side. The reference state for the gasifier assumes a profile that varies from 800 to 850 °C. This profile is motivated by the fact that the bed material entering the unit is colder and will heat up as the gasification process progresses.

Combustion

The velocity field is very low in a BFB combustor since the bubbling bed itself has a net velocity of zero across the bed. The only thing that can cause a very low field is the ash removal. To simulate this, an outlet flow equal to the inlet flow of ash was set.

The assumed temperature profile in the combustor is linearly decreasing from 850 °C at the inlet to 800 °C at the outlet. The inverse shape when compared to the gasifier is motivated by the fact that the combustion of volatiles takes place near the feed port which causes a rapid increase in temperature in that area.

CLC

For CLC, the velocity field is also coupled to the fuel feed rate since the bed material consists of oxygen carrier whose flow is directly proportional to the fuel input through the oxygen demand of the fuel. An oxide of manganese, Mn_3O_4, was chosen as an oxygen carrier and physical properties were taken from the work of Mattisson (Mattisson, Lyngfelt & Leion 2009). To be able to keep the sub model for combustion, which assumed that there is gaseous oxygen around the fuel particle, a special type of CLC is considered. It is known as CLOU, Chemical-Looping with Oxygen Uncoupling. As the name suggests, the oxygen carrier releases the oxygen which can then react with the fuel. (Mattisson, Lyngfelt & Leion 2009)

The mass flow of bed material is calculated based on the assumption that 80 % of the oxygen in the oxygen carrier is released. The concentration of oxygen around the fuel particle is calculated based on equilibrium partial pressures from Mattiasson. (Mattisson, Lyngfelt & Leion 2009)

3 Method

A literature study was carried out in order to gain a basic understanding of the problem at hand and to learn how other authors have handled the difficulties inherent in the task. The study included both the functionality of a BFB unit and mathematical modelling of BFB units in general.

A one-dimensional mathematical model has been formulated based on the governing equations found in the literature study and given in Section 2. This model was developed step-wise from the most fundamental processes and adding complexity as the work progressed.

The model was then validated with experimental data and tested for stability before some different design cases for gasification, combustion and CLC were run.

4 Results and discussion

4.1 Study of the model

A number of simulations were performed to test the stability of the model and some of its parameters.

4.1.1 Mesh independency

An important property of any CFD calculation is mesh independency. The solution should not depend on the size of the computational cells. For a coarse mesh, the solution will naturally not be as exact as for a finer mesh. At some point, the mesh is sufficiently fine so further refinements will not affect the overall solution, within a certain tolerance level. At this point, mesh independency is said to be achieved.

To evaluate the model for grid independency, a series of simulations were run for gasification of wood in the Chalmers gasifier. The number of cells was varied between 7 and 300 which correspond to a cell length of 257 and 6 mm respectively.

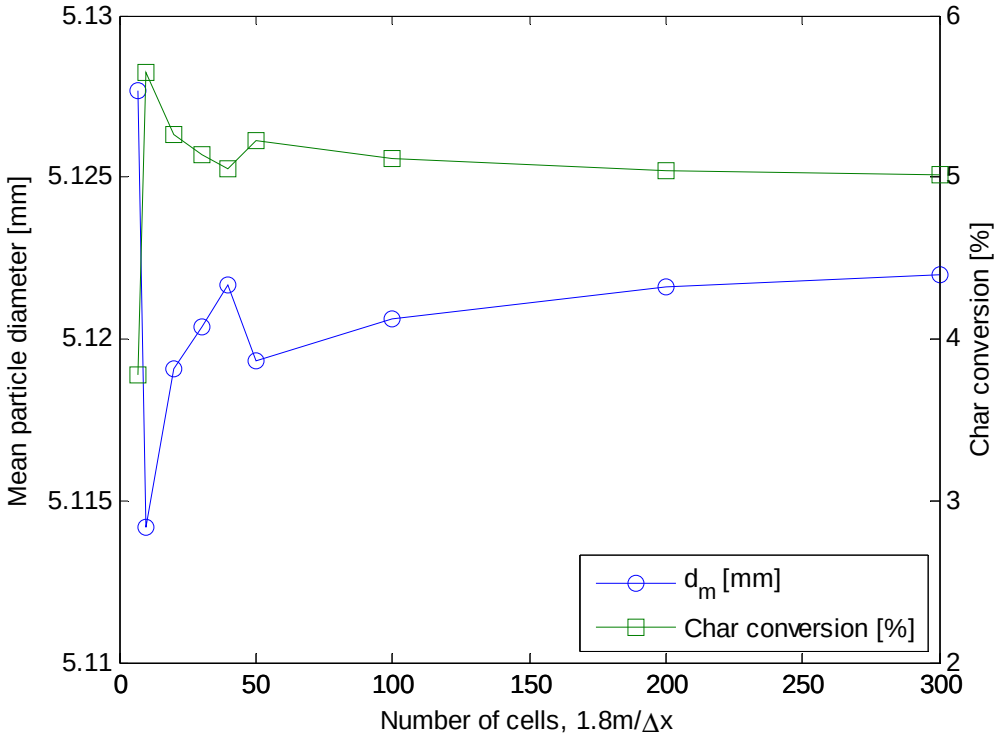

Figure 6 Test of mesh dependency for gasification of wood in the Chalmers gasifier.

As can be seen in Figure 6, the solution saturates towards a stable value as the number of cells are increased. Beyond 100 cells, which correspond to a cell length of 18 mm, little change is observed in the solution. Furthermore, the computational time is heavily dependent on the mesh resolution and the step from 100 cells to 200 cells increased the time to run the model from the order of tens of minutes to several hours. Based on these results, 100 cells were deemed enough to reach grid independency.

4.1.2 Number of particle size classes

To find how the solution depends on the number of particle size classes, a series of simulations were run on the reference cases for gasification, combustion and CLC of wood and coal. Each case was tested with 10, 20, 30, 50, 100, 150, 200, 250, 300, 400, 500 and 1000 size classes. For gasification, combustion and CLC of coal, the results changed little with more than 300 classes. This is illustrated by the case of combustion of coal which can be seen in Figure 7 and Figure 8. Based on these findings, 300 size classes were chosen to be the reference case. The difference between 150 and 1000 size classes is small but there is still a difference in the smallest available particle diameter, which decreases as the number of size classes increases, thus the additional classes will give a more accurate value for the mean particle size in the outlet.

There were two reasons not to divide the particles into even more classes. Since the difference in diameter between the largest sizes grows slower as the number of particles size classes increases, a number of numerical precision errors are introduced in Matlab. The computational time is strongly affected by the number of particle size classes. For the case of coal combustion, there was a difference in computational time of a factor of six between 10 and 300 particle size classes, and 16 and 57 in the same scale in the case of 500 and 1000 size classes respectively.

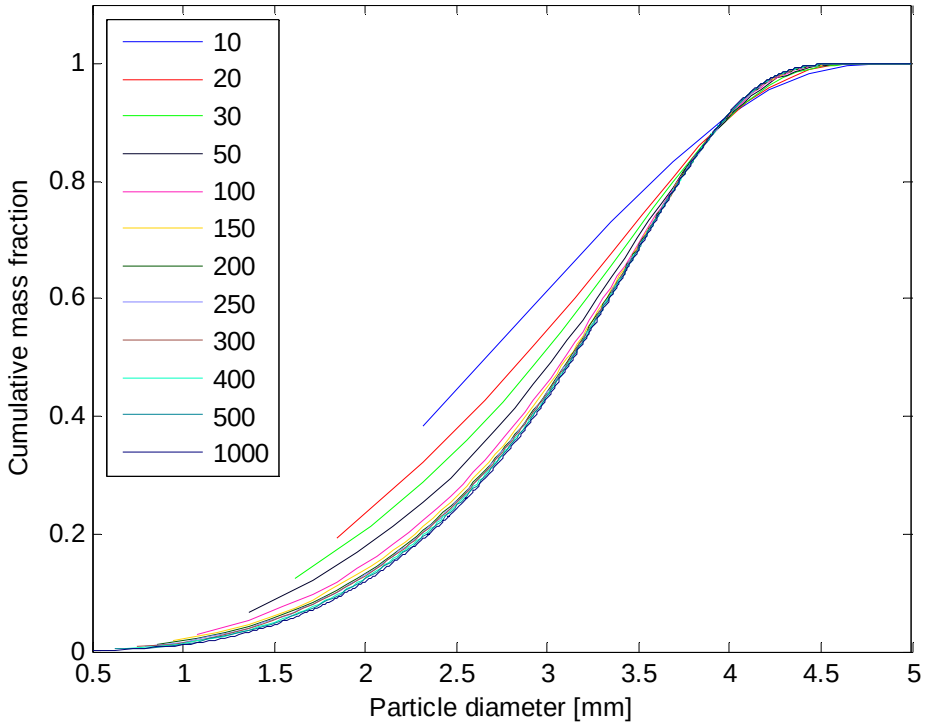

Figure 7 Cumulative outlet char PSD for different number of particle size classes for combustion of coal.

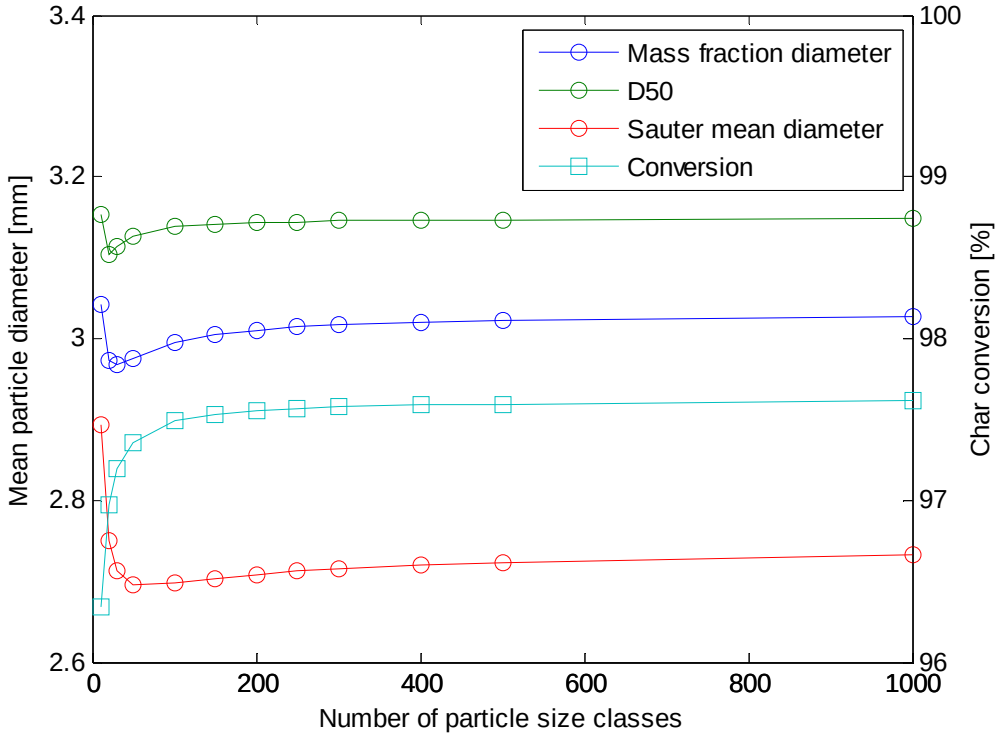

Figure 8 Mean particle diameter in the outlet and conversion for a number of different particle size classes for combustion of coal.

The results from Figure 8 were compared to the case where only one particle size was allowed.

Table 5 Comparison between the results from 300 particle size classes and one particle size class.

Number of particle size classes	Conversion [%]	Mean particle diameter [mm]
300	97.58	3.02
1	87.29	5

As Table 5 shows, the inclusion of particle size classes has a very large effect on the results. The conversion is 10 percentage points lower if no particle size development is included in the model. The mean particle diameter will be the same as the input diameter if no particle size development is allowed.

In one specific case, combustion of wood, there was no convergence as the number of size classes was varied. As shown in Figure 9 and Figure 10, there is no clear correlation between the cumulative mass fraction, mean particle diameter, conversion and the number of particle size classes. The problem is clearly shown if one compares the lines for 1000 and 2000 size classes in Figure 9.

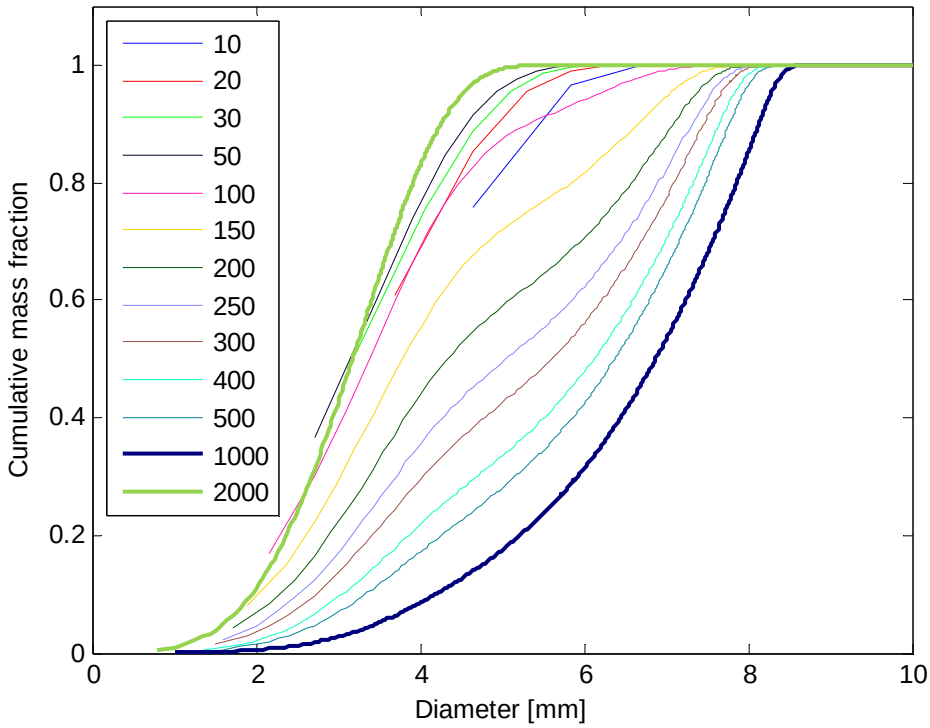

Figure 9 Cumulative mass fraction for different number of particle size classes in the outlet for combustion of wood.

The source of this problem was identified to be a combination of the combustion model and the primary fragmentation model. If the secondary fragmentation model was disabled, a similar result was received. If both fragmentation models were removed, a converging result, similar to the one showed in Figure 7 and Figure 8, was found. Another case where the primary fragmentation model for wood was exchanged for the primary fragmentation for coal once again gave results similar to the ones with the fragmentation model for coal. These results show that the problem is not in the fragmentation model in itself but a combination of the fragmentation and the combustion model.

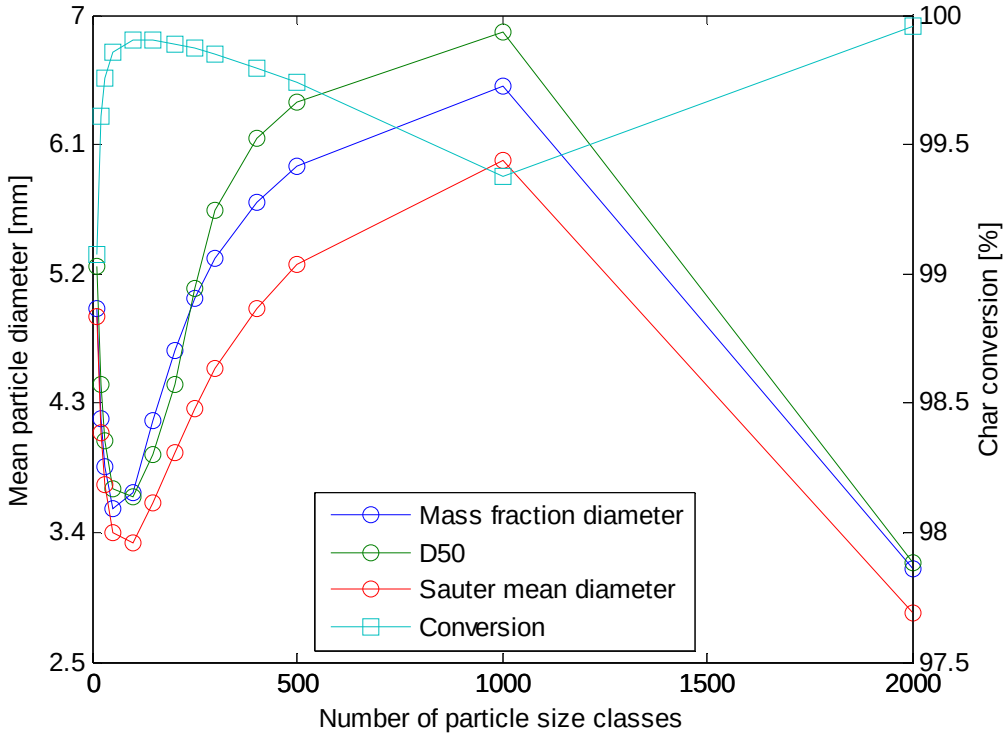

Figure 10 The mean particle diameter in the outlet and conversion for a number of different particle size classes for combustion of wood.

4.1.3 Mean particle diameter

The particle size distribution in the outlet stream from the unit is an important design metric. In a gasifier, the amount and size of the particles in the outlet provides a direct measure of the overall conversion in the unit. In a combustion chamber, the outlet flow of char is supposed to be as low as possible because any char in the outlet is a loss of energy. In a CLC unit, the particle properties in the outlet of the reactor are of great importance because char must not enter the air reactor.

The three different ways to calculate a mean particle diameter in the outlet described previously were compared to find the most suited to characterize the properties of the outlet.

Figure 11 shows the outlet cumulative particle size distribution for gasification of coal. Because of the high activation energy of coal and the short residence time, very little char conversion takes place in the gasifier. Therefore, most of the particle size development is due to the primary fragmentation. Not all particles undergo fragmentation which gives a bi-modal particle size distribution of char. One unfragmented mode with a large diameter and one fragmented mode with a small diameter. There is a gap between the two fractions where there is little or no char, seen as a plateau in Figure 11. This leads to an inherent weakness of the D50 mean diameter. Due to the way it is defined, it will give a very large diameter for the case of gasification of coal.

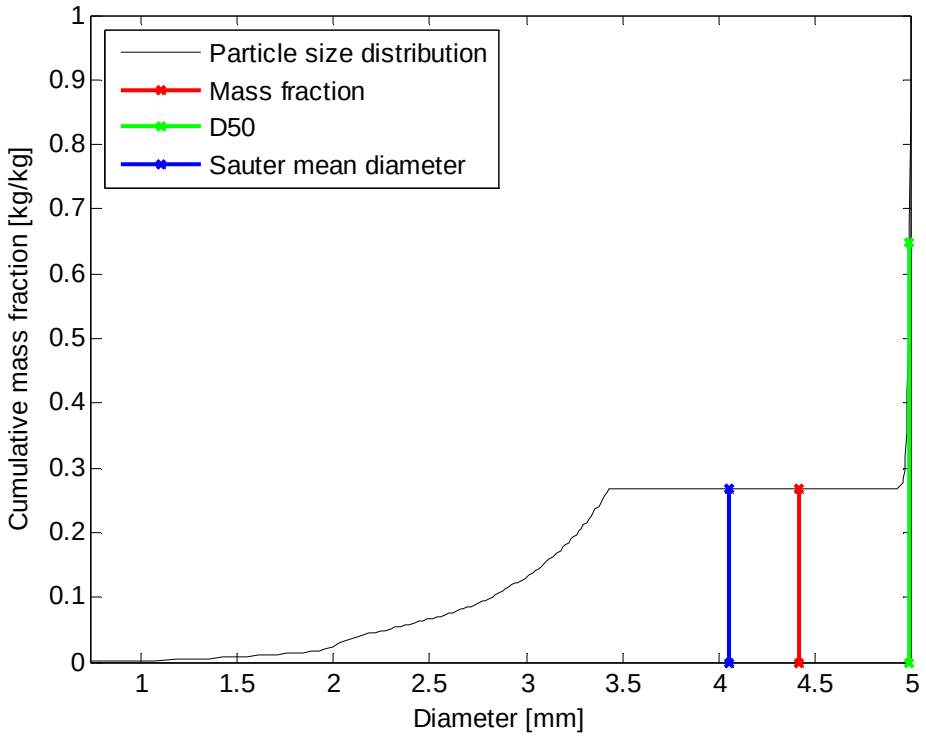

Figure 11 Cumulative mass fraction in the outlet for gasification of coal with the three different mean particle diameters marked.

Figure 11 also reveals another weakness of D50 that is related to the way it is calculated in the model. It can be clearly seen that the D50 is not in fact at 0.5 as it should. This is caused by the fact that the cumulative curve is very steep so even a small numerical error in the interpolation can lead to a large error in the estimation of D50. In the specific case, D50 is calculated to be 4.9879 mm which corresponds to a point on the cumulative curve of 0.65. If a linear approximation between the data points as is used in the figure is assumed, a D50 of 4.9821 mm is found. The difference between the two mean diameters is 0.12 % but result in a difference of 15 percentage units on the cumulative curve. In this case, the numerical error will not affect the diameter itself because of the steep curve. If the point corresponding to 0.5 on the cumulative curve had been on the plateau on the other hand, then a small numerical error would have a large effect on the mean diameter. Based on these findings, D50 is deemed to be unsuitable for characterization of the outlet particle composition.

Because of the way the Sauter mean diameter is calculated, see equation (45), smaller particles have a greater impact on the result than larger ones. This can give variations in the Sauter mean diameter depending on the resolution of the finer intervals. Figure 12 shows the cumulative mass fraction for combustion of wood which has a relatively high fraction of smaller particles due to low activation energy, a long residence time and heavy fragmentation, both primary and secondary. It shows that the Sauter mean diameter is smaller than the other two. If the fraction of smaller fragments had been larger, the effect would have been even more pronounced. For this reason, the Sauter mean diameter is also deemed to be unsuitable for characterization of the outlet particle composition.

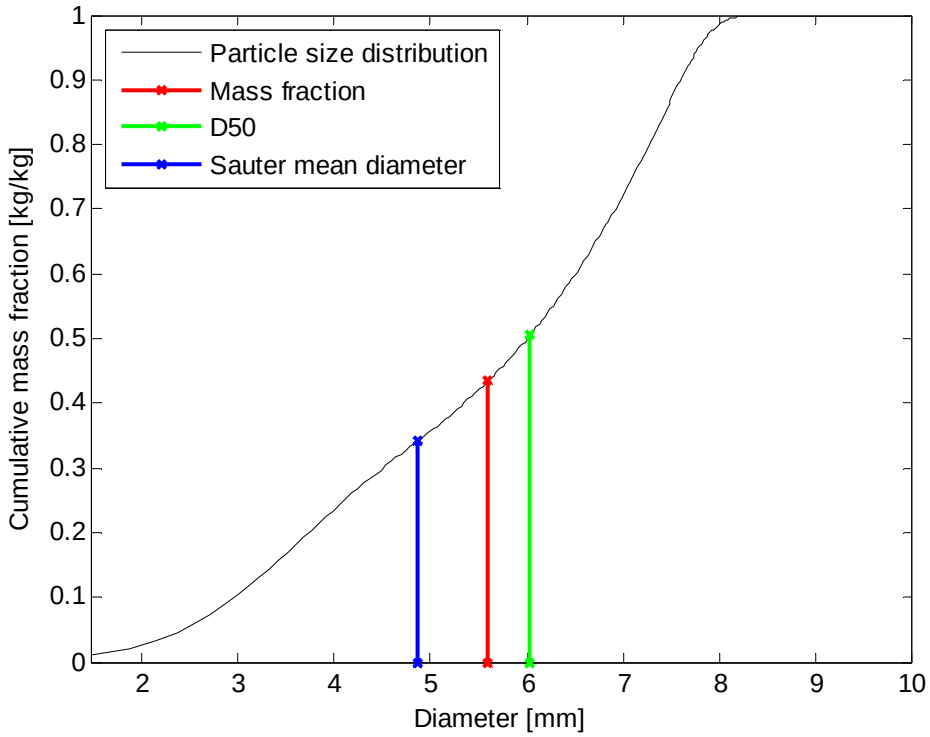

Figure 12 Cumulative mass fraction in the outlet for combustion of wood with the three different mean particle diameters marked.

The mean diameter based on mass fraction $\bar{d}_m$, as seen in equation (44), has been the most stable and will be used to characterize the outlet particle size distribution.

4.2 Sensitivity analysis

To evaluate the stability of the model, a series of sensitivity analyses was performed on the variables that were deemed to have the greatest effect on the result.

4.2.1 Error tolerance level

Three simulations were run for the Chalmers gasifier with wood as fuel with an error tolerance level for the total mass balance of 10^{-3}, 10^{-4} and 10^{-5} and with the total char conversion and the mean particle diameter being used as indicators. The results are shown in Table 6.

Table 6 Sensitivity analysis of the tolerance level in the convergence criterion in the mass balance in the reference case for gasification of wood.

	Tolerance = 10^{-3}	Tolerance = 10^{-4}	Tolerance = 10^{-5}
Conversion [%]	5.0131	5.1007	5.1095
$\bar{d}_m$ [mm]	5.1242	5.121	5.1207

Between the tolerance level of 10^{-3} and 10^{-4}, a percentage difference of 1.72 % for the char conversion and 0.06 % for mean particle diameter was found. The corresponding numbers for the percentage difference between 10^{-4} and 10^{-5} was 0.16 % and 0.006 %

respectively. Based on this, a tolerance level of 10^{-4} was deemed enough to find a convergent solution since a lower level would not affect the result in any significant way.

4.2.2 Temperature profile

The effect of a change of the temperature profile used as input was performed by comparing the reference temperature profile, which is set to be a linearly increasing profile from 800 °C to 850 °C, with one higher and one lower. The higher temperature profile was set to be 850-900 °C and the lower was set to be 750-800 °C. A fourth case with a constant temperature of 825 °C was also run.

As can be seen in Figure 13, the model is very sensitive to a change in temperature. The resulting char conversion was 2.4 %, 5.1 % and 10 % for the three runs. The overall conversion varies by a factor of two as the temperature profile is changed by 50 °C. For comparison, the simulation with a constant temperature of 825 °C yielded a char conversion of 5.7482 % and a mean diameter in the outlet of 5.1165 mm.

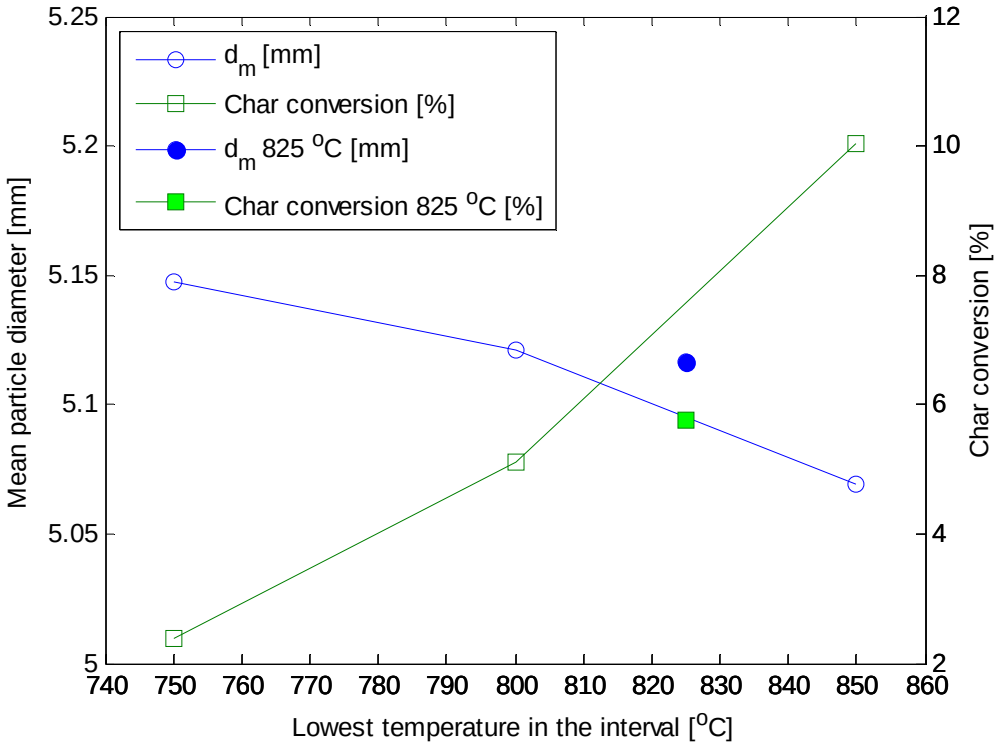

Figure 13 The effect of temperature on the mean diameter in the outlet and the overall char conversion for the Chalmers gasifier at the reference case.

The high temperature dependency of the char conversion stems from the temperature dependency of the reaction rate. Based on these findings, the assumption of a linear temperature profile might be wrong and an energy balance to calculate a more realistic temperature profile is needed.

4.2.3 Activation energy

The sensitivity of the activation energy was evaluated by comparing the reference value of 160 kJ/mol with values that were 10 % higher and lower than the reference value which corresponds to an activation energy of 176 and 144 kJ/mol respectively.

Figure 14 shows a clear dependency of the activation energy where a 10 % increase causes a 61.9 % decrease in conversion and a 10 % decrease in the activation energy causes an increase of 158.2 %. The simulation shows that the result is highly dependent on the activation energy.

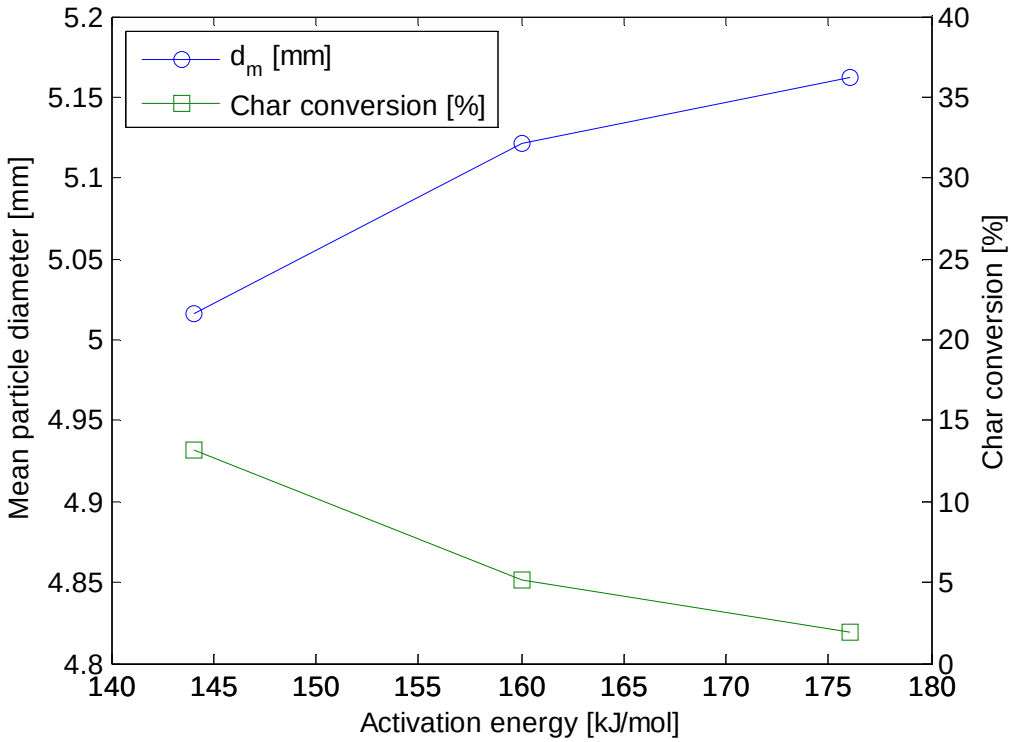

Figure 14 The effect of the activation energy on the mean particle diameter in the outlet and the overall char conversion for the Chalmers gasifier at the reference case.

To further analyse the effect of the kinetics, a sensitivity analysis of the effect of the pre-exponential factor as well as the activation energy was performed. In the combustion model, the pre-exponential factor is a function of the activation energy so to test which part has the largest effect on the result, this coupling was removed by setting the value of the activation energy to the reference value of 160 kJ/mol and the value of the pre exponential factor was adjusted by 10 % in both directions. To test the effect of the activation energy, the pre-exponential factor was assumed to be a constant that did not depend on the activation energy. Instead, the activation energy was set to the reference value when calculating the pre-exponential factor and only the activation energy in the Arrhenius equation was varied by 10 %.

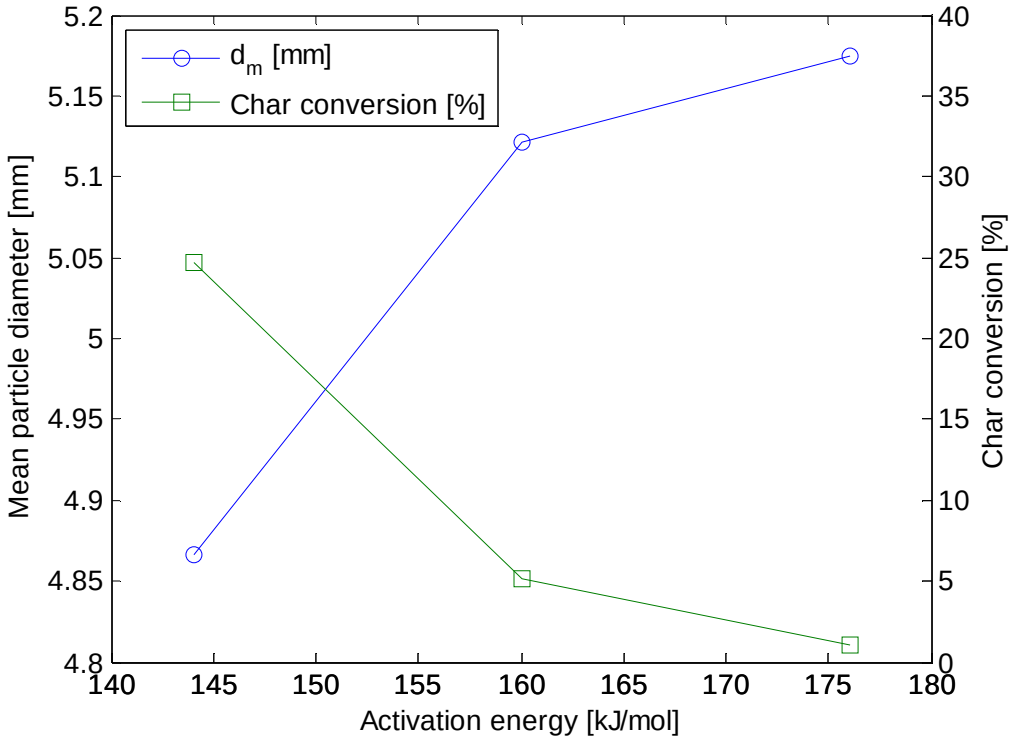

Figure 15 The effect of the activation energy on mean particle diameter and char conversion with the pre-exponential factor held constant.

As can be seen in Figure 15, the activation energy has a large impact on the result. A decrease of 10 % in the activation energy yields a fivefold increase in char conversion.

In contrast to activation energy, the pre-exponential factor acts as a dampener to this effect. Figure 16 shows that an increase in activation energy will result in a small increase in conversion. Overall, the result is not very sensitive to a change in the pre-exponential factor.

However, the char conversion model used in this work has a pre-exponential factor that is a function of the activation energy as can be seen in equation (28) where an increase in the activation energy give an increase in the pre-exponential factor which in turn would give an increase in the conversion. So this dependency acts as a dampening factor to the overall reaction rates dependency on the activation energy.

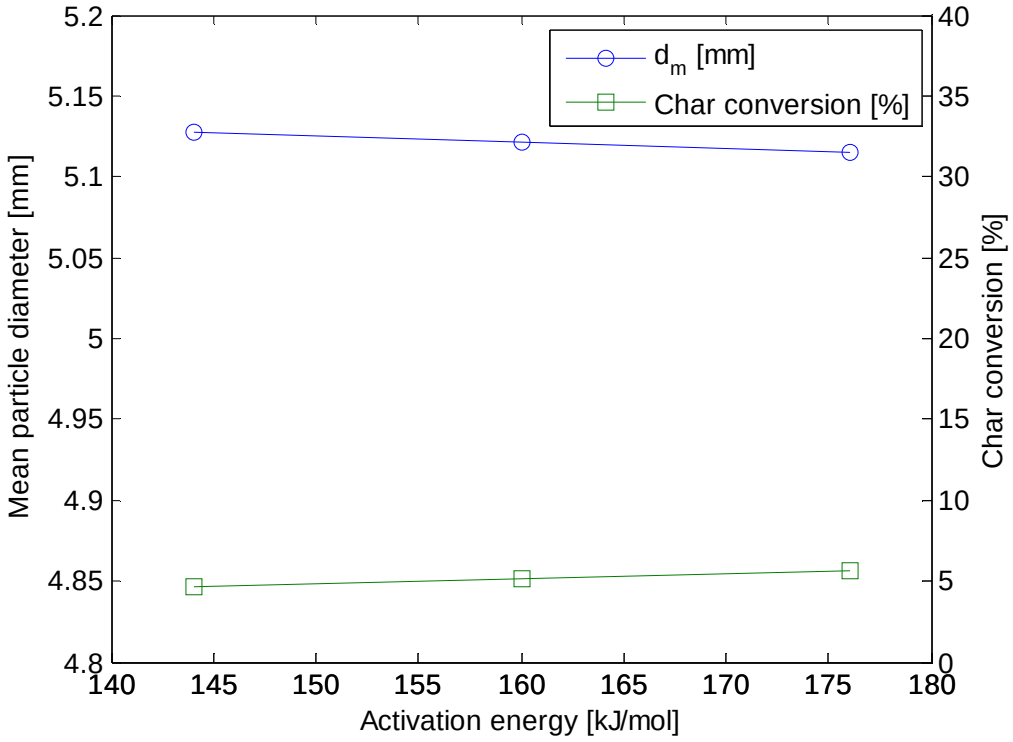

Figure 16 The effect of the pre-exponential factor on mean particle diameter and char conversion with the activation energy held constant.

4.2.4 Attrition

The results of simulations with and without attrition were compared for three cases as shown in Table 7.

Table 7 Comparison of char conversion and mean particle diameter in the outlet for five different cases using reference conditions.

	Conversion with attrition [%]	Conversion without attrition [%]	Mean diameter with attrition [mm]	Mean diameter without attrition [mm]
Gasification of wood	5.1007	4.984	5.121	5.1205
Gasification of coal	0.72065	0.70222	4.4114	4.4113
Combustion of coal	97.578	97.5751	3.0167	3.0162

If attrition is removed from the model, a reduction in conversion can be seen. It ranges from 2.56 % for gasification of coal to 0.003 % for combustion of coal. The mean diameter is however consistently increasing when attrition is removed. This effect is cause by the fact that the reaction rate constant is larger for smaller particles so the

kinetics is faster and the attrition is treated as a reaction so the overall kinetics is further increased. Since the reaction is now faster for the lower particle classes, more small particles are completely converted which shifts the mean diameter towards the larger particles even though the conversion is increased.

To test the sensitivity of the numerical value of the attrition constant, a simulation was run with the constant set to one of the larger and one of the lower values available in the literature and the results were compared to the reference state of gasification of coal. (Chirone 1991)

Table 8 The results from three simulations comparing a high and a low value for the attrition constant with the reference state for gasification of coal.

	Conversion [%]	Mean diameter [mm]
$k = 5 \cdot 10^{-7}$	0.978	4.4121
$k = 3.33 \cdot 10^{-8}$	0.72065	4.4114
$k = 3.33 \cdot 10^{-9}$	0.70406	4.4113

Table 8 shows that changing the attrition constant by an order of magnitude have a small effect on the results. Based on these results, an exact numerical value of the attrition constant is not important and a value of $3.33 \cdot 10^{-8}$ is taken for the simulations shown hereafter.

4.2.5 Fragmentation

To test the effect of fragmentation, three tests were run on combustion of coal. One with both primary and secondary fragmentation, one with only primary fragmentation and one with no fragmentation at all. For gasification of wood, the limited char residence time prevents secondary fragmentation, so it is not included in the gasification model. The results can be seen in Table 9.

Table 9 Char conversion and mean particle diameter for gasification of wood and combustion of coal with different fragmentation behaviour.

	Gasification of wood		Combustion of coal	
	Conversion [%]	Mean diameter [mm]	Conversion [%]	Mean diameter [mm]
Primary and secondary fragmentation	-	-	97.578	3.0167
Only primary fragmentation	5.1007	5.121	97.5604	3.0203
No fragmentation	2.9943	9.8967	96.891	3.1175

The introduction of a fragmentation model does not have a large effect on the combustion of coal since the residence time for the reference case is long enough to reach an almost complete conversion anyway. The addition of fragmentation creates more small particles at the start of the combustion process which increases to overall combustion and thus the overall char conversion. In the case of gasification, the introduction of a fragmentation model has a big impact on the result. The overall conversion is not greatly affected but the change in mean diameter in the outlet is large. Without any primary fragmentation to break up the fuel particles into smaller pieces, the char conversion is the only process that drives the particle size development. With the low overall conversion of the gasifier, this effect is highly visible and illustrated in Figure 17.

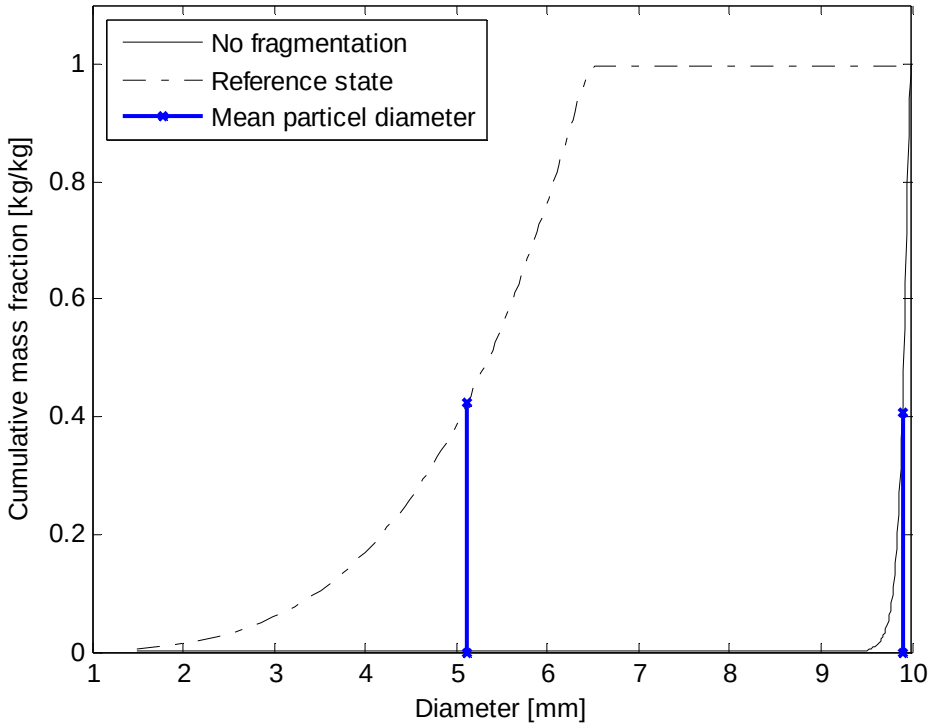

Figure 17 Cumulative outlet char PSD for gasification of wood, with and without primary fragmentation. The mean particle diameters for each simulation are marked.

The addition of a model for fragmentation is very important to fully characterize the char composition in the outlet.

4.2.6 Slip factor for fuel velocity

To evaluate the impact of the velocity slip factor, α, three tests were performed in which it decreased linearly from one for the smallest char particles to 0.3, 0.6 and 1 respectively for the largest.

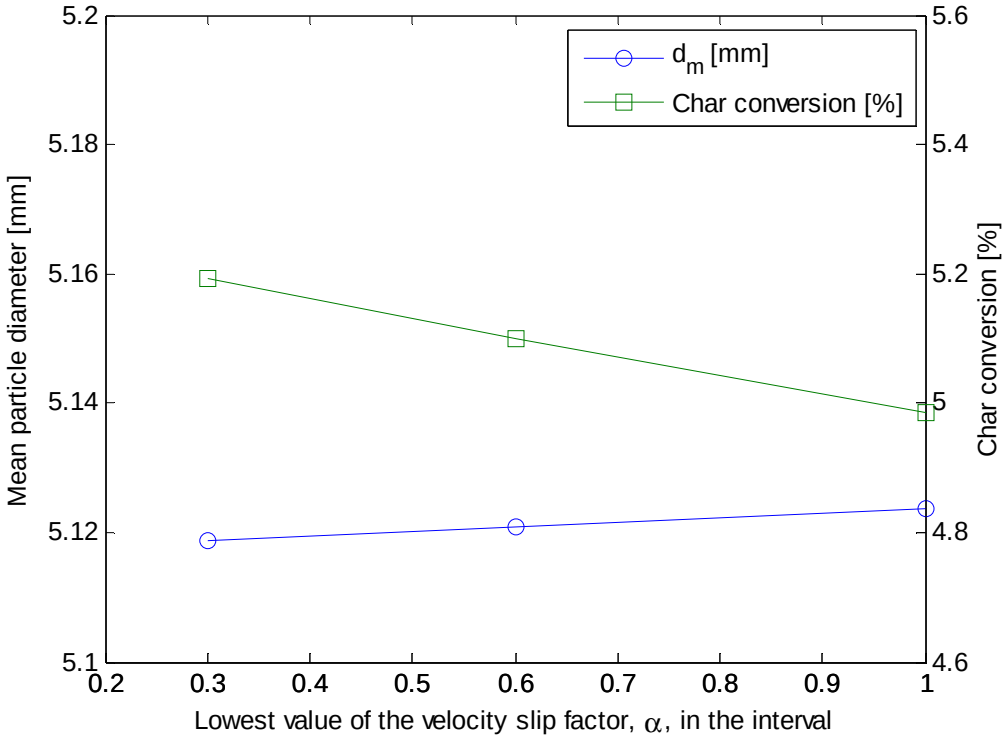

Figure 18 The influence of the velocity slip factor on the char conversion and mean particle diameter in the outlet for the reference case of gasification of wood.

Figure 18 shows a weak correlation between α and the conversion and mean particle diameter.

A similar test was performed for combustion of coal to evaluate the effect of the velocity slip factor on a case where dispersion is the dominating transport process.

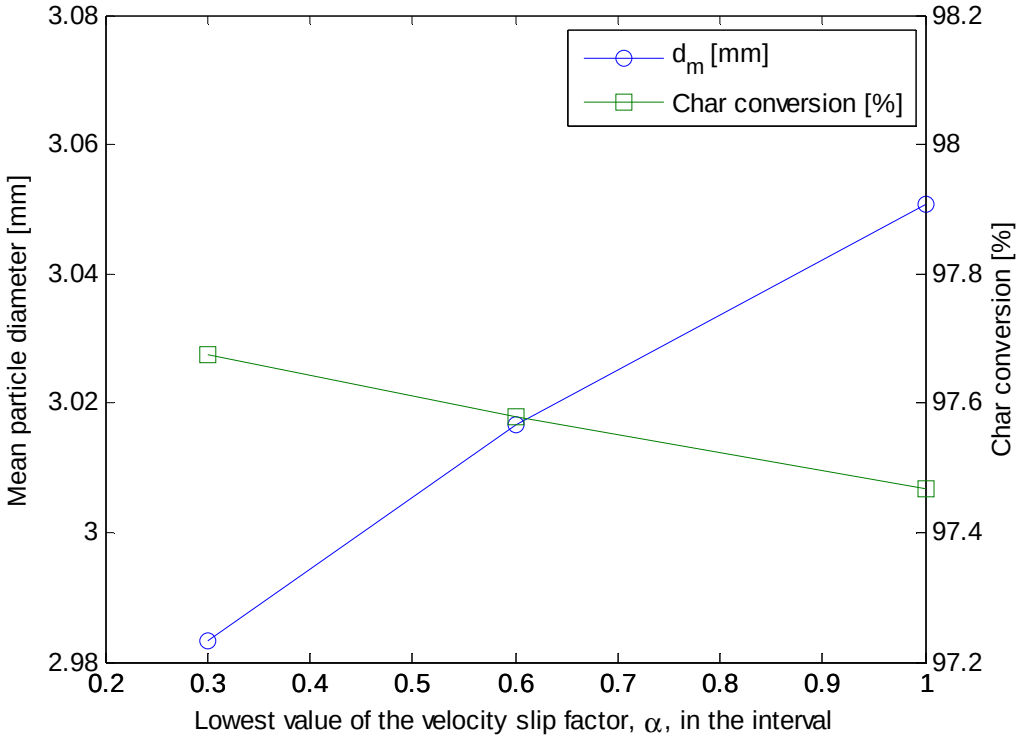

Figure 19 The influence of the velocity slip factor on the char conversion and mean particle diameter in the outlet for combustion of coal.

Figure 19 shows similar results with a small effect on the char conversion but a larger effect on the mean particle diameter. This is caused by the fact that a low value of the velocity slip factor corresponds to a long residence time for larger particles which in turn leads to higher conversion rate. The mean particle diameter is therefore more sensitive to a change in the overall particle size distribution for the combustor.

4.2.7 Dispersion coefficient

To test the sensitivity on the dispersion coefficient, two applications were considered. One case with gasification of wood and another case with combustion of coal.

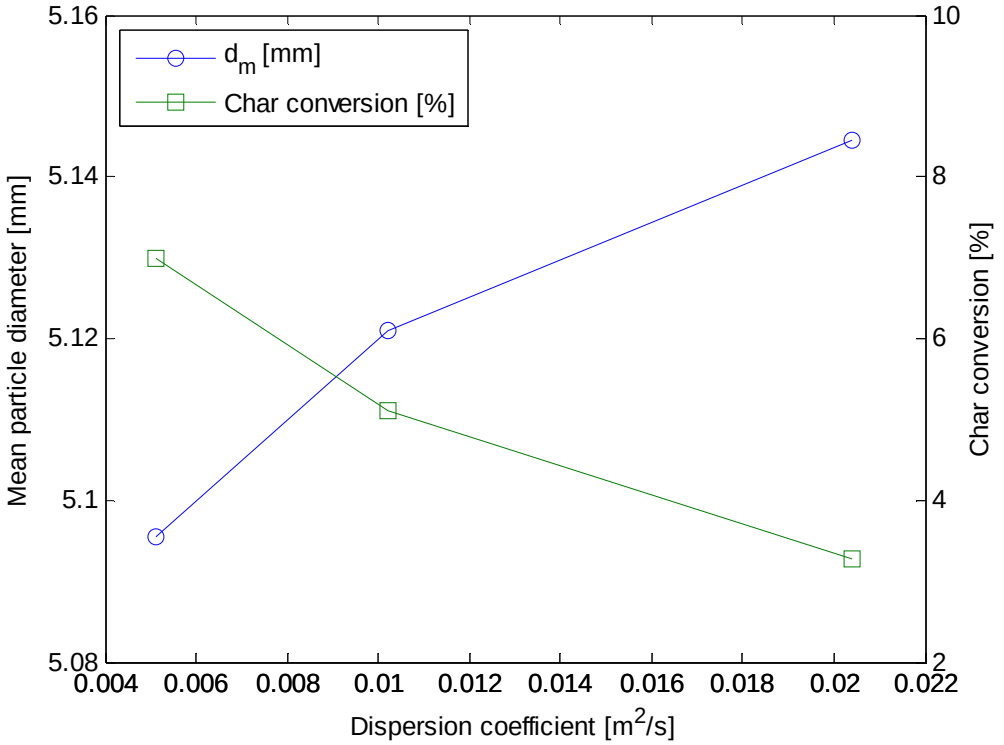

Figure 20 Effect of the dispersion coefficient on the mean particle diameter and overall char conversion for gasification of wood.

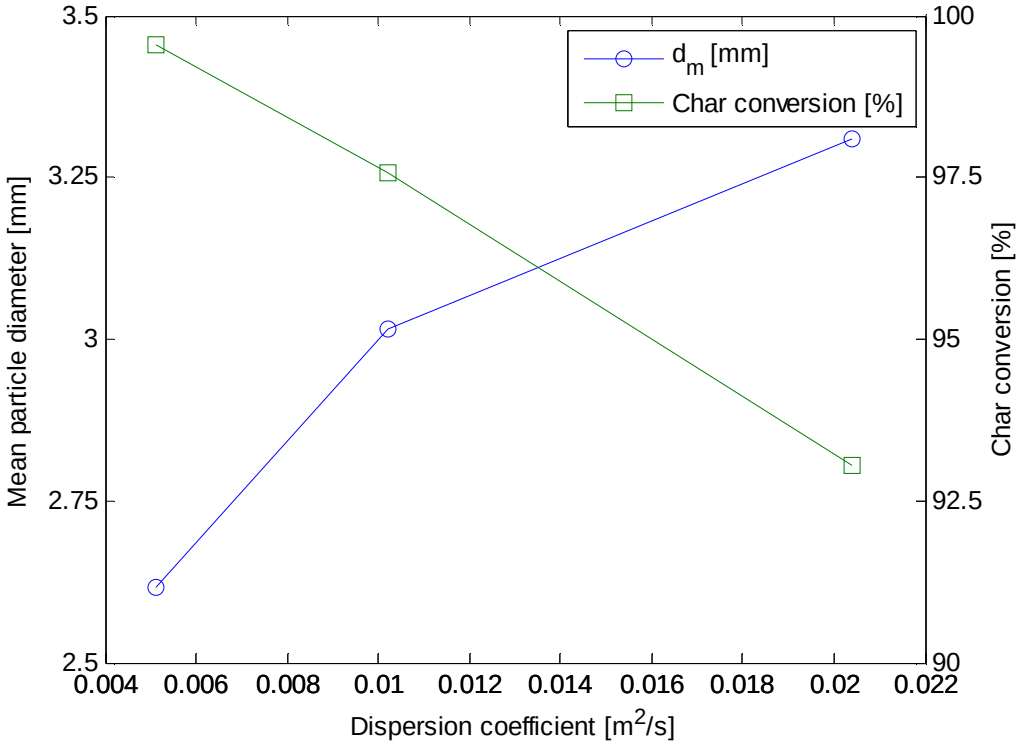

Figure 21 Effect of the dispersion coefficient on the mean particle diameter and overall char conversion for combustion of coal.

In qualitative terms, both cases behave similarly as shown in Figure 20 and Figure 21. Quantitatively, the decrease in char conversion for a four-folded increase in the dispersion coefficient was of 114.27 % and 7.01 % for wood gasification and coal combustion respectively. This is caused by the lowering of the residence time as the dispersion coefficient increases.

4.2.8 Particle size distribution

To test the effect of the particle size distribution in the fuel feed, two cases with a normal distribution of the fuel particle diameter corresponding to one narrow and one wide distribution was compared to a case with mono-sized fuel. The two normal distributions are both centred on the 30th particle size class which corresponds to a mean fuel particle diameter of 9.667 mm. To vary the normal probability density function, two different values of the standard deviation was assumed of 10 and 80 respectively and the mean size was held constant. This corresponds to a distribution that spans 66 particle size classes between 9.22 and 10 mm for σ equals 10 and a distribution that spans 284 particle size classes between 3.84 and 10 mm for σ equals 80.

Table 10 Effect of fuel PSD on conversion and mean outlet fuel size.

	Conversion [%]	Mean diameter [mm]
Mono-size	5.12	5.1206
9.22 – 10 mm, $\sigma = 10$	5.1186	5.1229
3.84 – 10 mm, $\sigma = 80$	5.1152	5.1269

Table 10 shows that there was little difference between the three different cases. The difference in char conversion between the narrow normal distribution and a mono-sized feed was 0.027 % and the difference between the narrow and the wide normal distribution was 0.066 %. The difference in outlet mean particle diameter was 0.045 % and 0.078 % respectively. Based on this, the assumption of a mono-sized fuel feed is valid.

4.3 Modelling results

The model calculates a concentration profile for char, volatiles, moisture and ash for the length of the modelled unit as show in Figure 22 and Figure 24.

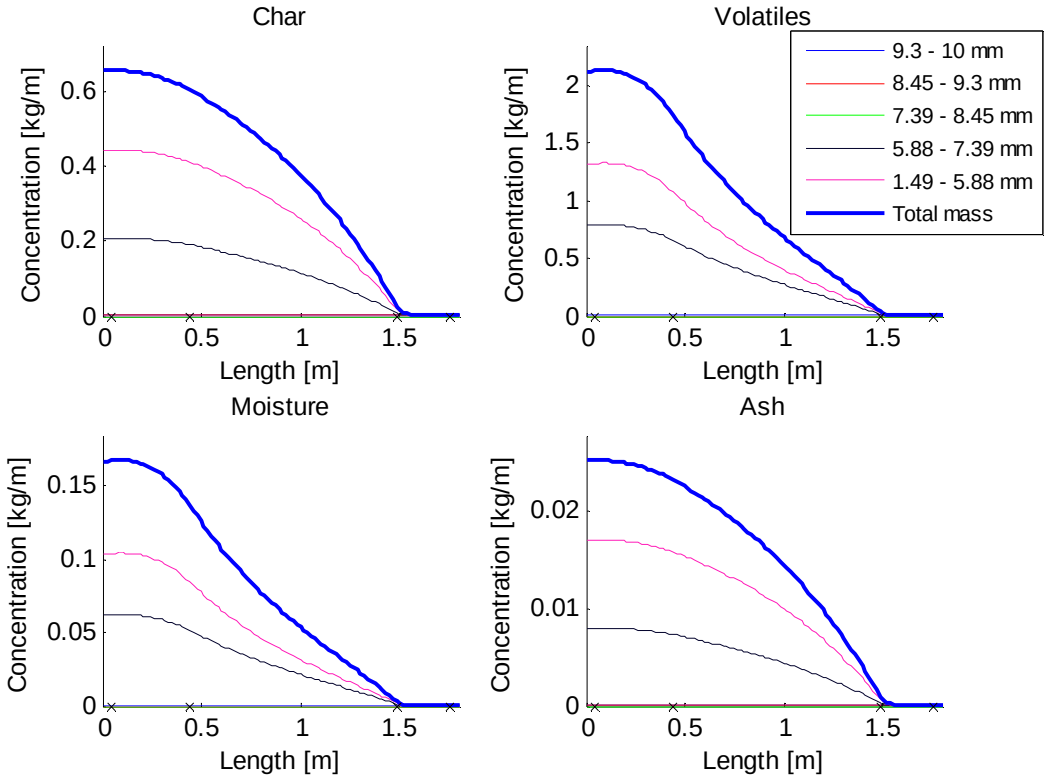

Figure 22 Concentration profiles for char, volatiles, moisture and ash in the Chalmers gasifier using wood as fuel. The feed and outlet location is marked with x.

Figure 22 show a very steep concentration gradient even though the overall conversion is low. The char conversion is 5 % for the gasifier but there is still a relatively low concentration of char by the outlet. Because the mass transfer in the gasifier is dispersion dominated, the gradient is steeper over the length of the unit. This can be compared to the convection dominated CLC of coal with a fuel reactor of the same size as the Chalmers gasifier which yields an overall char conversion of 12.25 % at 100 MW as shown in Figure 23. Here, the concentration decreases much less over the length of the unit only to drop rapidly at the outlet because the dispersion is much lower.

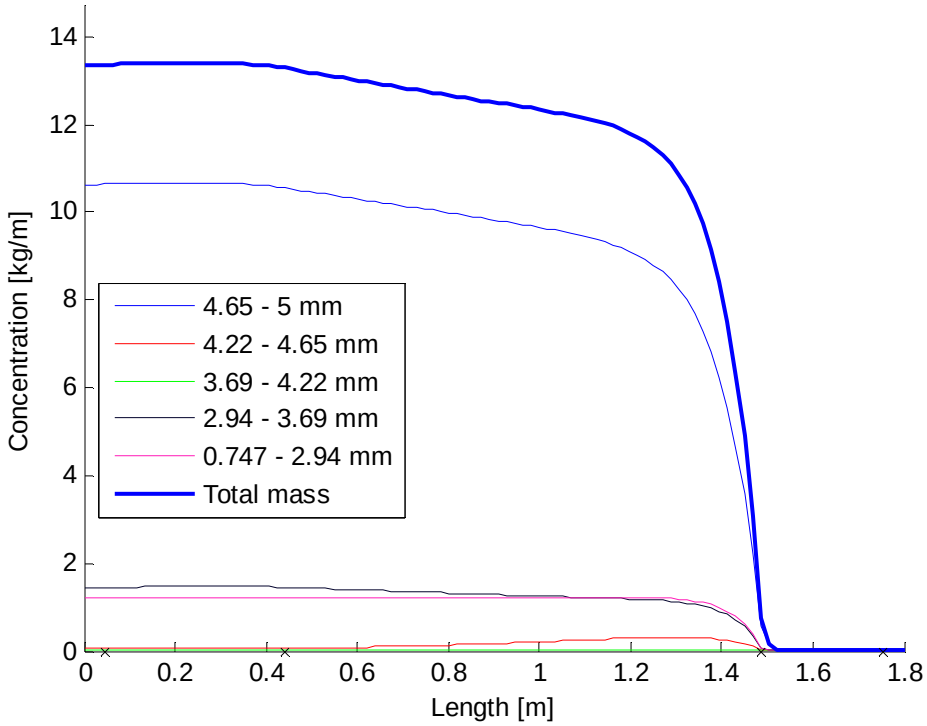

Figure 23 Concentration profile for char from coal in a 100 MW CLC fuel reactor with the same dimensions as the Chalmers gasifier. The total char conversion is 12.25 %. The feed and outlet location is marked with x.

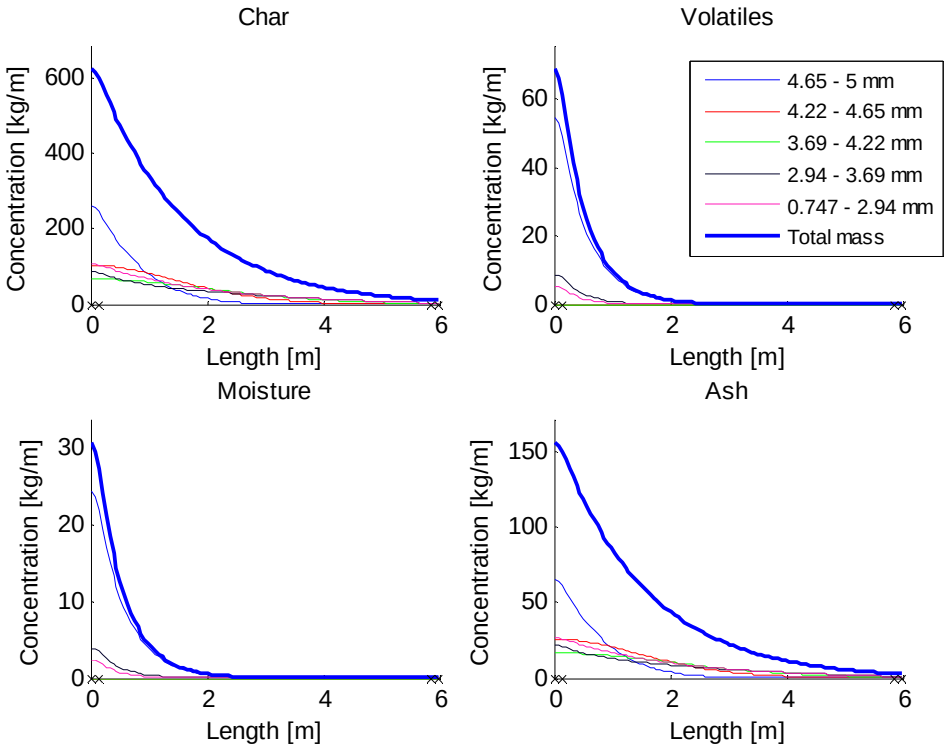

Figure 24 Concentration profiles for char, volatiles, moisture and ash for the combustion of coal in a 250 MW unit. The feed and outlet location is marked with x.

As can be seen in Figure 22, there are volatiles and moisture present throughout the length of the gasifier which means that the assumption that the transport of char, volatiles and moisture are independent might not be suitable for a unit with such low residence time. In contrast, Figure 24 show that the concentration of volatiles and moisture decreases quite rapidly after the inlet and most is gone after one third of the unit length.

4.4 Gasification

To evaluate the effect of the aspect ratio of the gasifier, a series of tests were run with the Chalmers gasifier as a base. The aspect ratio was varied over 15 steps from a square, i.e. aspect ratio of 1, to an aspect ratio of 10. The current gasifier design has an aspect ratio of 2.25. All other parameters such as fuel input and cross-sectional area were held constant. The cross-sectional area is 1.44 m^2 and the thermal input is 2MW, i.e. an cross-sectional specific loading of 1.3889 MW/m^2.

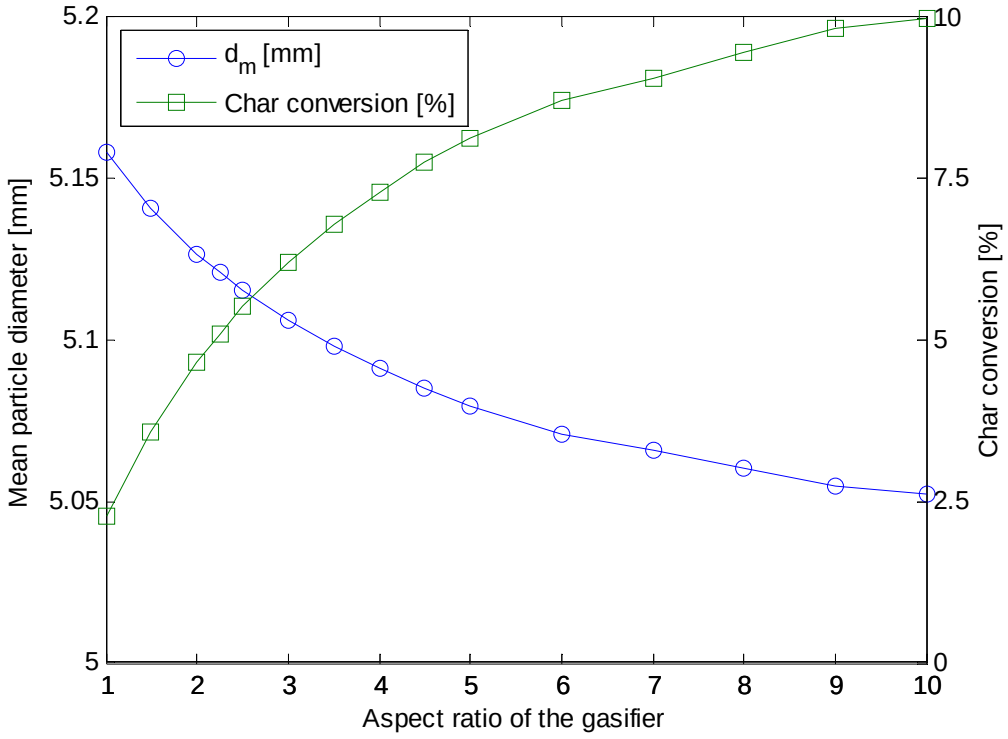

Figure 25 The mean diameter and char conversion for different aspects ratios based around the Chalmers gasifier.

As can be seen in Figure 25, the mean diameter and conversion are converging towards a specific value as the aspect ratio increases. These results indicate that a very long and narrow gasifier would be beneficial but there are obvious limitations which make an aspect ratio of 10 unfeasible. The test does however show that the efficiency of the Chalmers gasifier could be increased if the aspect ratio was longer. A small increase in aspect ratio from the current 2.25 to 3 would increase the char conversion by one percentage point.

The model was also used to evaluate the future GoBiGas gasifiers which have a rated power of 20 and 80 MW. They are assumed to have the same cross-sectional specific

loading as the Chalmers gasifier and all dimensions, including the size of inlet and outlet, are scaled to match the increased power. The calculated measurements and their associated aspect ratios are shown in Table 11.

Table 11 Measurements for each aspect ratio for the three gasifier cases. All lengths are in meters.

Ratio	1	1.5	2	2.25	2.5	3	3.5	4	4.5	5
Chalmers gasifier										
L	1.2	1.47	1.7	1.8	1.9	2.08	2.25	2.4	2.55	2.68
W	1.2	0.98	0.874	0.8	0.758	0.693	0.64	0.6	0.565	0.537
20 MW GoBiGas, demo scale										
L	3.79	4.65	5.37	5.69	6	6.57	7.1	7.6	8.05	8.5
W	3.79	3.1	2.68	2.53	2.4	2.2	2.03	1.9	1.79	1.7
80 MW GoBiGas, full scale										
L	7.59	9.3	10.73	11.38	12	13.15	14.2	15.16	16.1	16.97
W	7.59	6.2	5.37	5.06	4.8	4.38	4.06	3.8	3.58	3.4

The following figures show the results from those simulations. As the length of the unit increases, so does char conversion, which also increases quite drastically with size. At 80 MW, the overall char conversion is ten times higher which can be seen if Figure 26 and Figure 28 are compared. Overall, the same general trends can be seen regardless of the size of the gasifier.

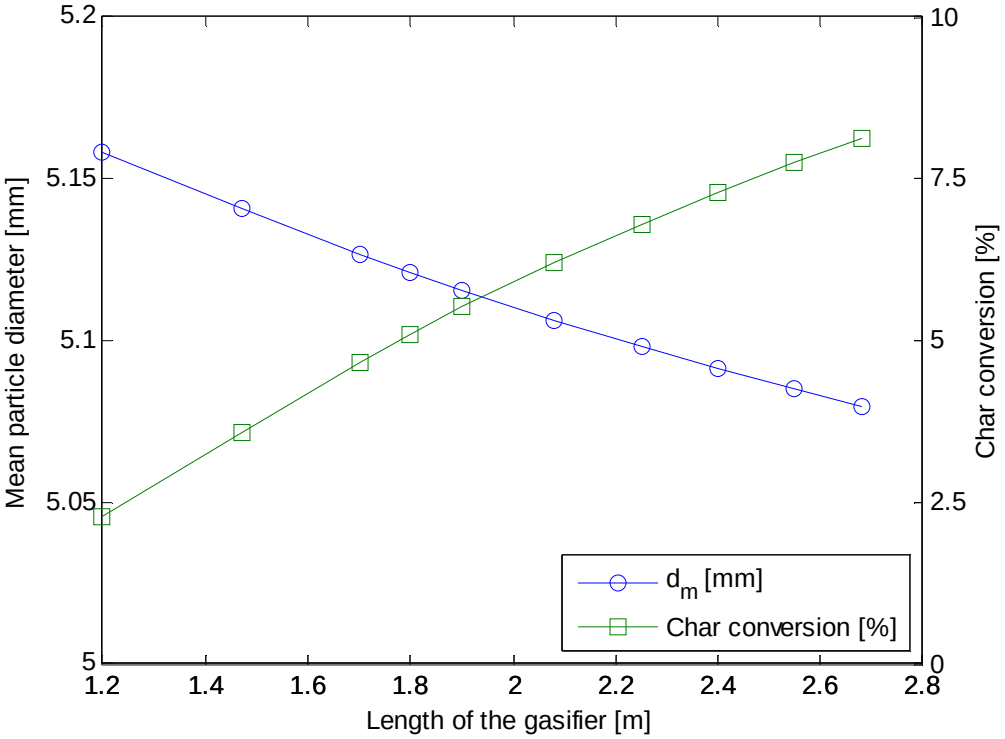

Figure 26 The char conversion and mean particle diameter in the outlet for the Chalmers gasifier as the aspect ratio is varied.

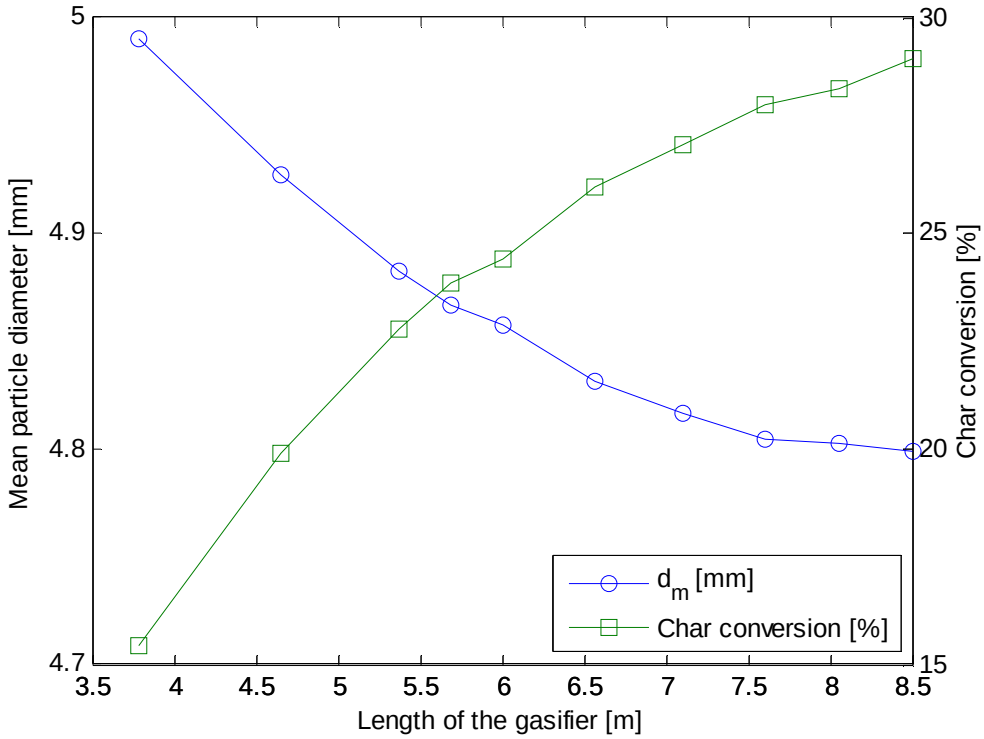

Figure 27 The char conversion and mean particle diameter in the outlet for the simulated 20 MW GoBiGas gasifier for different aspect ratios.

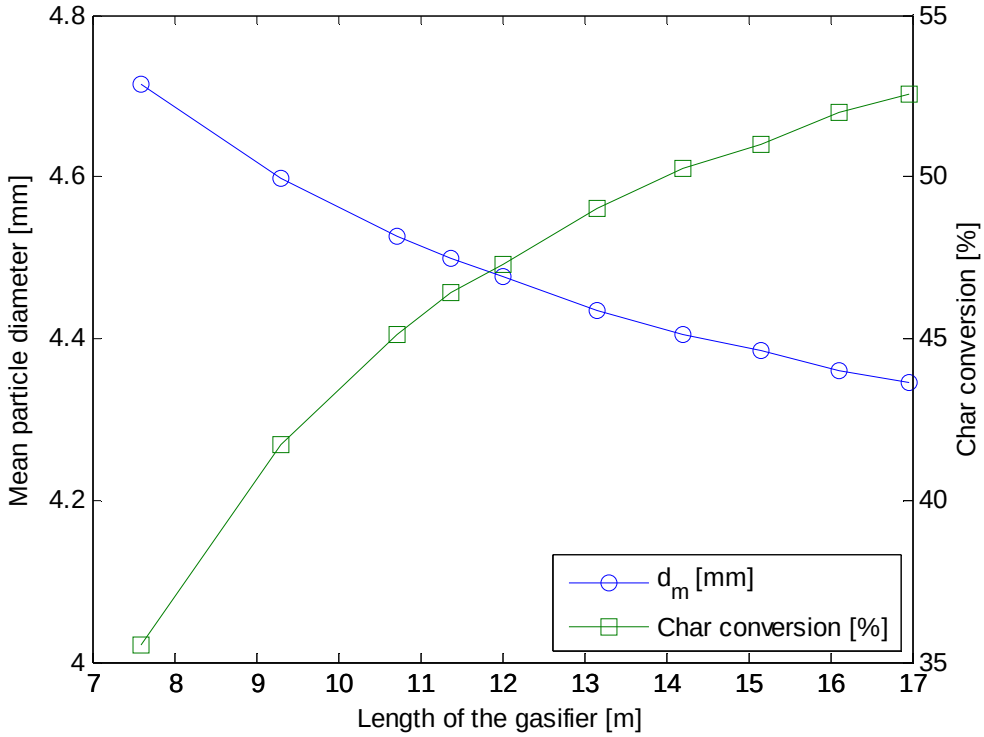

Figure 28 The char conversion and mean particle diameter in the outlet for the simulated 80 MW GoBiGas gasifier for different aspect ratios.

4.5 Combustion

To evaluate the model for use for combustion of coal, a series of tests were run to compare char conversion and mean particle size in the outlet for different sizes of combustors. For this test, a cross-sectional specific loading of 5 MW/m^2 was assumed for all cases. The combustor was then assumed to be square up to the critical length of 4.75 meters. Beyond that, the length was set to 4.75 meters and the width was increased to the necessary area. The calculated dimensions are shown in Table 12.

Table 12 Boiler properties for the combustor with constant cross-sectional specific loading.

Thermal power [MW]	10	50	100	250	500
Area [m^2]	2	10	20	50	100
Length [m]	1.414	3.162	4.472	4.75	4.75
Width [m]	1.414	3.162	4.472	10.526	21.053

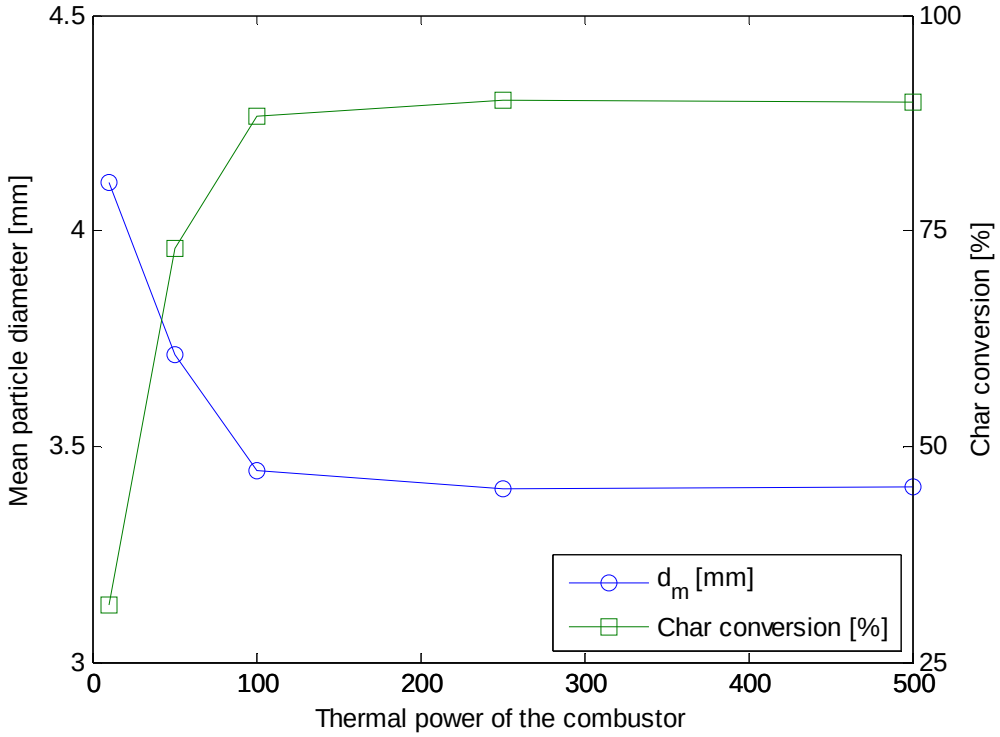

Figure 29 Char conversion and mean particle diameter for different thermal power for combustion of coal. Constant cross-sectional specific loading (W/m^2) is assumed.

As shown in Figure 29, the conversion increased up to the point of the critical length. After that, as the boiler gets wider, the conversion and mean particle diameter on the opposite side to the fuel feeding become constant.

4.6 CLC

To evaluate the cross-sectional shape of a CLC unit, the length and width of a simulated fuel reactor was varied between 1 and 10 meters, in one meter increments. The cross-sectional specific loading was assumed to be 4 MW/m^2.

The sizes of the inlet and outlet as well as the bed height were scaled to the same relative size and height as in the Chalmers gasifier.

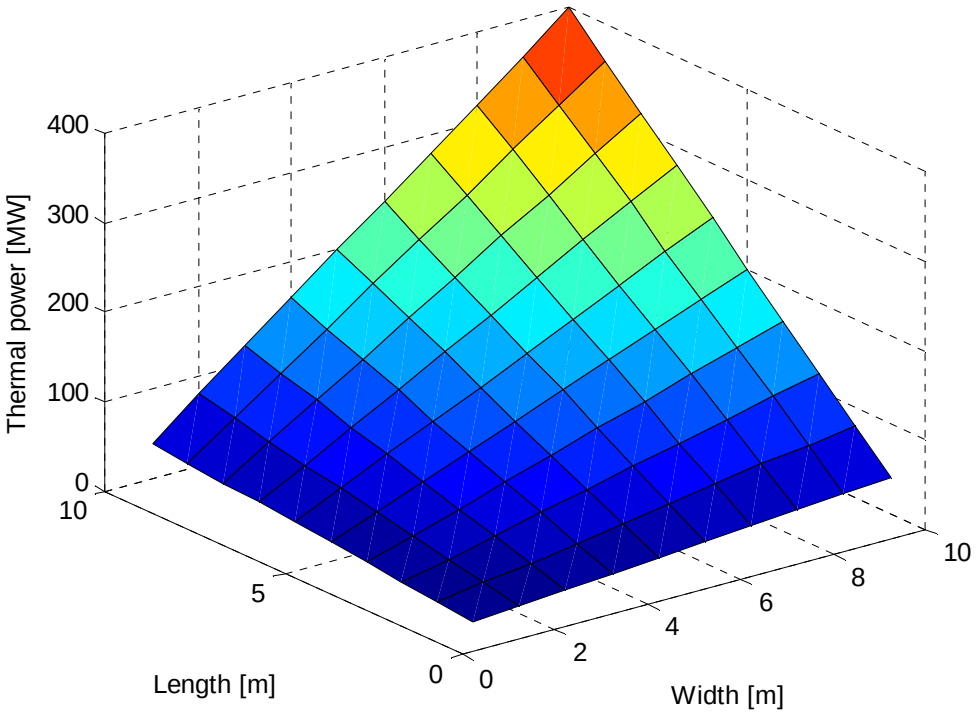

Figure 30 Thermal power for different sizes for a CLC fuel reactor.

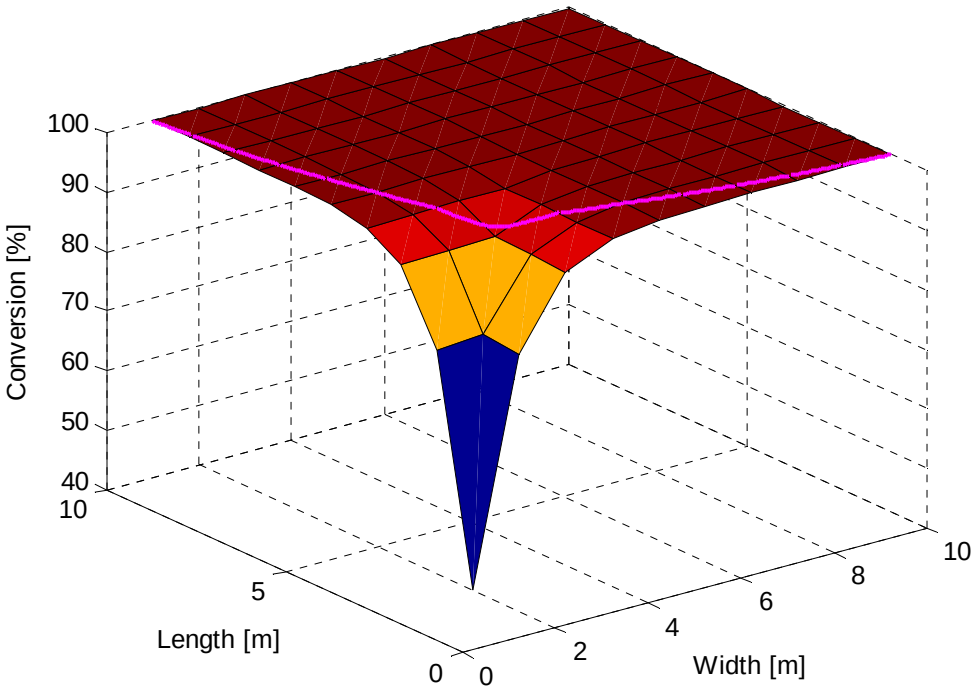

Figure 31 Char conversion for different sizes for a CLC fuel reactor. The purple line indicates a power of 40 MW. The figure is mirrored along the diagonal.

As can be seen in Figure 31, char conversion is constant for all sizes as long as they have passed the critical length of 3 meters as given by equation (30). The mean particle diameter shows a similar, but inverted pattern as can be seen in Figure 32.

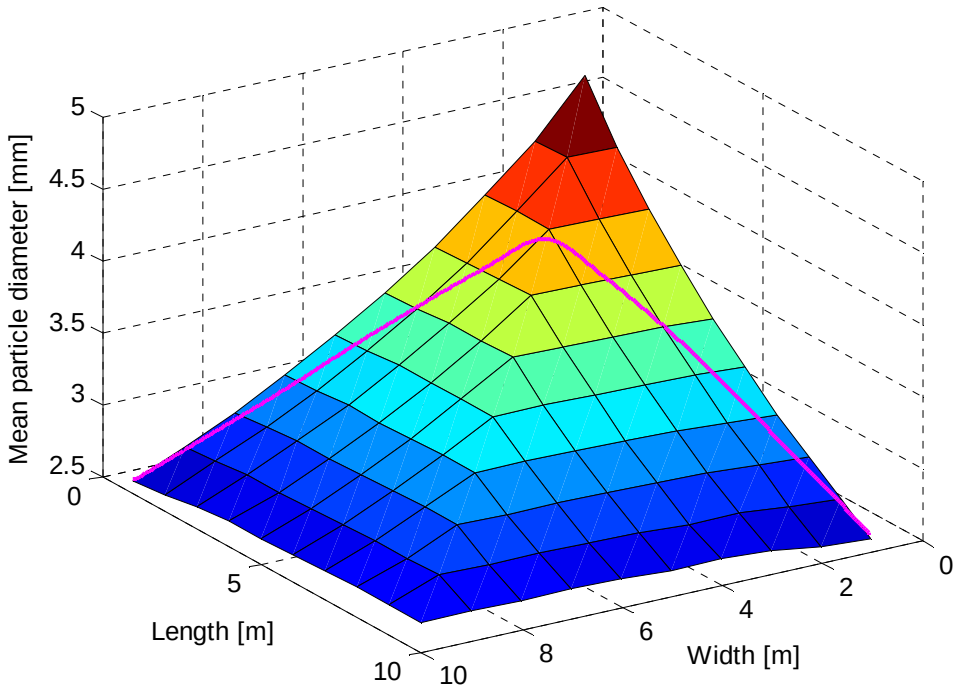

Figure 32 The mean particle diameter in the outlet for different sizes for a CLC fuel reactor. The purple line indicates a power of 40 MW. The figure is mirrored along the diagonal. Please note that compared to Figure 30 and Figure 31; the axes are inverted to make the figure clearer.

Based on these results, the highest conversion and smallest mean particle diameter in the outlet are achieved with a long and narrow reactor because of the longer residence time. Such a design is however not feasible for technical reasons. Following the purple line which corresponds to a power of 40 MW in Figure 31 and Figure 32, it can be seen that changing the aspect ratio from a square unit to a unit with an aspect ratio of 10 decreases the mean char particle diameter in the outlet from 3.97 mm to 2.59 mm and increases char conversion from 96.43 % to 99.99 %.

5 Conclusions

The inclusion of particle size classes and development in the modelling showed to be of relevance, increasing char conversion for a case with combustion of coal from 87.29 % to 97.58 %.

The inclusion of fragmentation in the modelling is shown to be very important in order to fully characterize the char composition in the outlet.

The model shows that fuel-specific properties used as input, specially the activation energy, have a strong influence of the results. This sets strong requirements on fuel characterization in order to make a quantitative use of the modeling

The model does not converge for certain combinations of inputs, such as combustion of fragmenting wood.

Based on a scale up simulation of the Chalmers gasifier, the future 80 MW GoBiGas gasifier will be able to reach a char conversion around 50 %.

Modelling has shown that changing the aspect ratio from a square unit to a unit with an aspect ratio of 10 yields an increase of char conversion from 96.43 % to 99.99 % and from 2.26 % to 9.98 % for CLC and gasification respectively. The mean char particle diameter in the outlet will decrease from 3.97 mm to 2.59 mm and from 5.16 mm to 5.05 mm respectively.

6 Further work

- Include a heat balance to obtain the temperature field and thus provide a better input to the modelling of the reaction kinetics.
- Expand the model to 3D.
- Solve the problem of combustion of fragmenting wood yielding different particle size distributions in the outlet depending on the number of particle size classes used.

7 Bibliography

Arena, U, D'Amore, M & Massimilla, L 1983, 'Carbon Attrition During the Fluidized Combustion of a Coal', *AIChE Journal*, January 1983, pp. 40-49.

Chirone, R 1991, 'Comminution of Carbons in Fluidized Bed Combustion', *Prog. Energy Combust. Sci.*, 1991, pp. 297-326.

Chirone, R, Salatino, P & Massimilla, L 1989, 'Secondary Fragmentation of Char Particels During Combustion In a Fluidized Bed', *Combustion and Flame*, 1989, pp. 79-90.

Energi, G, *Göteborg Energi*, viewed 15 June 2013, <http://www.goteborgenergi.se/English/Projects/GoBiGas__Gothenburg_Biomass_Gasification_Project>.

Larsson, J & Olsson, J 2013, 'Modelling and Optimization of Fuel Conversion in an Indirect Bubbling Fluidized Bed Gasifier', Master's Thesis, Department of Energy and Environment, Division of Energy Technology, T2013-389, Chalmers University of Technology, Göteborg.

Mattisson, T, Lyngfelt, A & Leion, H 2009, 'Chemical-looping with Oxygen Uncoupling for Combustion of Solid Fuels', *International Journal of Greenhouse Gas Control*, no. 3, pp. 11-19.

Mörtstedt, S-E & Hellsten, G 2005, *Data och diagram*, 7th edn, Liber AB, Malmö.

Scala, F & Chirone, R 2006, 'Combustion and Attrition of Biomass Chars in a Fluidized Bed', *Energy & Fuels*, 2006, pp. 91-102.

Sudhakar, DR, Reddy, KS, Kolar, AK & Leckner, B 2008, 'Fragmentation of Wood Char in a Laboratory Scale Fluidized Bed Combustor', *Fuel Processing Technology*, 2008, pp. 1121-1134.

Thunman, H 1997, *Loading and Size Distribution of Fuel in a Fluidized Bed Combustor*, Chalmers University of Technology, Göteborg.

Thunman, H 2012, *Combustion Engineering*, Department of Energy and Environment, Chalmers University of Technology, Göteborg.

Thunman, H & Seemann, M 2009, 'First Experiences With the New Chalmers Gasifier', *20th International Conference on Fluidized Bed Combustion*, Xi'an.